doi.org/10.36721/PJPS.2026.39.7.191.1

Integrated analyses identify key genes related to Qingyihuaji formula for pancreatic adenocarcinoma treatment based on network pharmacology combined with bioinformatics

Jintao Han[1], Fuchu Qian[2,3] and Jiemin Shi[1]*

[1]Department of Traditional Chinese Medicine, Huzhou Central Hospital, Affiliated Central Hospital, Huzhou Normal University, No.1558 Sanhuan North Road, Huzhou, Zhejiang, China.

[2]Department of Precision Medicine, Huzhou Central Hospital, The Fifth School of Clinical Medicine of Zhejiang Chinese Medical University, No.1558 Sanhuan North Road, Huzhou, Zhejiang, China.

[3]Huzhou Key Laboratory of Precision Medicine Research and Translation for Infectious Diseases, Huzhou Central Hospital, Affiliated Central Hospital, Huzhou Normal University, No.1558 Sanhuan North Road, Huzhou, Zhejiang, China.

Abstract: **Background**: Traditional Chinese medicine QingYiHuaJi formula (QYHJ) has anti-tumor effect in Pancreatic adenocarcinoma (PAAD). However, the potential mechanism and key targets of QYHJ have not been fully elucidated. **Objectives**: The aim of this study was to explore the underlying mechanisms and key targets of QYHJ in PAAD treatment. **Methods**: The overlapping genes between the targets of QYHJ and the common differentially expressed genes (Co-DEGs) identified in PAAD were selected as potential QYHJ for PAAD-related genes. The protein-protein interaction (PPI) network analysis, functional enrichment and pathways analyses were performed. ROC curve and Cox regression model were used to evaluate the diagnostic and prognosis value. Correlation between hub genes and immune cell infiltration were further analyzed. **Results**: A total of 9 hub genes (PTGS2, BCL2L1, ICAM1, MET, NQO1, MMP3, NFATC1, CCNB1, ERBB3) were identified. These hub genes were linked to inflammation, oxidative stress and apoptosis related signaling pathways. ROC analysis showed that 8 hub genes may serve as potential diagnostic markers. Survival analysis indicated that 6 genes (BCL2L1, CCNB1, ERBB3, MET, MMP3 and NFATC1) were closely related to prognosis of the PAAD patients. Cox regression analysis demonstrated that the model developed using the hub gene signature exhibited strong predictive capacity for clinical outcome. ICAM1, MET, NQO1 and ERBB3 were associated with infiltration of Th2 and Th17 immune cells. The low-risk group exhibited better drug sensitivity. **Conclusion**: These hub genes related to QYHJ have diagnostic value and may serve as potential prognostic and drug sensitivity biomarkers for PAAD.

Keywords: Bioinformatics; Network pharmacology; Pancreatic adenocarcinoma; Prognosis; Qingyihuaji formula

Submitted on 19-03-2025 – Revised on 24-11-2025 – Accepted on 01-12-2025

INTRODUCTION

Pancreatic adenocarcinoma (PAAD) is a highly aggressive tumor characterized by a low survival rate (Khalaf *et al*., 2021; Klein, 2021). Its poor prognosis results from aggressive behavior, treatment resistance and the absence of early diagnostic methods. Surgical resection remains the primary treatment for early-stage PAAD; however, over 80% of patients are diagnosed at an advanced stage and are ineligible for curative surgery (Park *et al*., 2021). Although chemotherapy and radiotherapy are established treatments, new treatment strategies have also been explored; nevertheless, there has been no significant improvement in overall survival rates among patients with metastatic disease in recent year (Siegel *et al*., 2023).

Traditional Chinese Medicine (TCM) has garnered significant interest from scholars due to its safety, effectiveness and low cost. This study aimed to improve the survival rate of PAAD patients through TCM therapy. The Qingyihuaji formula (QYHJ) was created by Professor Luming Liu based on the principle of "clear away heat and remove dampness." This approach has been utilized as a complementary therapy for PAAD treatment; it has demonstrated significant efficacy in enhancing the survival rates of individuals diagnosed with PAAD. QYHJ suppresses tumor proliferation and significantly improves survival rates in patients with advanced PAAD (Song *et al*., 2017). Mechanistically, the underlying mechanisms include downregulating immunosuppressive factors and metastasis-related genes, improving immune status, regulating the tumor microenvironment, reducing S phase cell proportion to inhibit tumor proliferation and modulating MAPK, PI3K-Akt and Foxo signaling pathways to suppress protein expression (Jing *et al*., 2020). However, owing to the complex compounds in TCM formulas, the mechanism and key targets of QYHJ in PAAD have not been fully clarified.

At present, network pharmacology is a novel tool used to study relationships among drugs, diseases and targets. It can predict and identify the basis of drug components, thereby aiding the understanding of mechanisms within drug effect networks (Liu *et al*., 2018; Qian *et al*., 2020). Using this method, it has been found that the DuhuoJisheng decoction (DHJSD) could improve intervertebral disc degeneration (IVDD) by regulating pyroptosis (Guo *et al*., 2023). It has been reported that the anti-gout mechanism of WuweiShexiang Pill (WSP) was related to the modulation of metabolic and biosynthetic pathways by combining network pharmacology and metabolomics analyses (Lang

**Corresponding author:* e-mail: shijiemin871007@126.com

et al., 2023). In addition, it has been identified key signaling pathway and the key targets of kaempferol using network pharmacology (Zhang *et al*., 2023). Recently, novel molecular targets were identified for intervention in PAAD from the Cancer Genome Atlas (TCGA) and Gene Expression Omnibus (GEO) databases. Therefore, integrating network pharmacology and bioinformatics analysis may be a novel approach to elucidate the targeting hub genes and mechanisms of QYHJ for PAAD therapy. This approach also provides a valuable opportunity to explore the pathogenesis of PAAD.

In this study, we aimed to identify target genes of the main components of QYHJ for PAAD treatment. Differentially expressed genes (DEGs) were identified by comparing normal samples to PAAD samples obtained from the GEO and TCGA databases. Subsequently, a network named "targets of QYHJ - targets of PAAD" was constructed to identify target genes shared by QYHJ components and the DEGs in PAAD. Hub genes were identified by analyzing protein-protein interactions (PPI) using the STRING database. Furthermore, bioinformatics was used to explore the functions and pathways of hub genes. Moreover, the diagnostic and prognostic value of the hub genes was assessed through receiver operating characteristic (ROC) curves and Cox regression analysis. The correlation between key genes and immune cell infiltration was investigated using single-sample gene set enrichment analysis (ssGSEA). Finally, we utilized drug susceptibility information derived from the Genomics of Drug Sensitivity in Cancer (GDSC) to predict the responsiveness of various subtypes of PAAD to anticancer drugs. This study will be helpful in exploring potential diagnostic and prognostic biomarkers and in understanding the mechanisms and key targets of QYHJ in PAAD treatment.

MATERIALS AND METHODS

Screening of active ingredients in QYHJ

QYHJ contains six traditional Chinese herbs: Amorphophallus Sinensis Belval (Sheliugu), Hedyotis Diffusae Herba (Baihuasheshecao), Scutellariae Barbatae herba (Banzhilian), Coicis Semen (Yiyiren), Alpinia Katsumadai Hayat (Baidoukou) and Gynostemmae Pentaphylli Herba (Jiaogulan). The compounds of each herb utilized in QYHJ were gathered from the Chinese Medicine Systems Pharmacology Database and Analysis Platform (Ru *et al*., 2014). The active ingredients of herbal in QYHJ were selected for further analysis according to oral bioavailability (OB) >30% and drug-likeness (DL) >0.18 (Lee *et al*., 2018) based on the pharmacokinetic properties of absorption, distribution, metabolism and excretion (ADME).

Prediction of targets in QYHJ

Prediction of the targets of QYHJ was carried out in the following steps. First, potential targets of the active ingredients from the six herbs were predicted using the TCMSP database. Then, these targets were translated into gene names by utilizing the UniProt Knowledgebase database (UniProtKB. Available at: https://www.uniprot.org. Accessed 15 May 2024).

PAAD datasets collection and processing

PAAD dataset (TCGA-PAAD) was downloaded using TCGAbiolinks package (version 2.36.0) from TCGA (https://portal.gdc.cancer.gov/). Following the removal of samples that did not contain clinical information, data were acquired from a total of 177 samples, which included 173 tumor samples (PAAD group) and 4 normal samples adjacent to cancer (normal group).

All data were normalized to the Fragments Per Kilobase per Million (FPKM) format. Sample information was obtained from the UCSC Xena database (Goldman *et al*., 2020). The TCGA-PAAD dataset was used as a test set.

PAAD datasets, GSE62452 and GSE57495, were acquired from the GEO database (Gene Expression Omnibus. Available at: https://www.ncbi.nlm.nih.gov/geo/, Accessed 15 May 2024) using the GEOquery package (version 2.76.0). GSE62452 is based on the GPL6244 platform, specifically the Affymetrix Human Gene 1.0 ST Array [transcript (gene) version] and comprises 69 PAAD and 61 normal samples. GSE57495 utilizes the GPL15048 platform, which corresponds to the Rosetta/Merck Human RSTA Custom Affymetrix 2.0 Microarray [HuRSTA_2a520709.CDF] and includes 63 PAAD tissue samples. All samples from these two datasets were selected for analysis. We used the SVApackage (version 2.2.0) to eliminate batch effects between the datasets and obtained a combined dataset (GEO-combined) used as the validation set; this combined dataset includes 132 PAAD samples and 61 normal samples.

Screening of differently expression genes

DEGs were analyzed in TCGA-PAAD and GEO-combined datasets using the limma package (version 3.64.1) (Ritchie *et al*., 2015). The screening criteria for DEGs were $|\log_2 FC| > 0$ and p-value< 0.05. Genes with $\log_2 FC > 0$ and p-value< 0.05 were categorized as upregulated, while genes with $\log_2 FC < 0$ and p-value<0.05 were categorized as downregulated. Volcano plots of DEGs in the TCGA-PAAD and GEO-combined datasets were generated. By intersecting the DEGs from these two datasets, we obtained common DEGs (co-DEGs) between the TCGA-PAAD and GEO-combined datasets.

Identification of QYHJ for PAAD-related genes

The gene set of QYHJ for PAAD-related genes was obtained by intersecting the screened QYHJ targets with Co-DEGs. Subsequently, a network of TCM-ingredients-targets was constructed. Heatmaps of TCGA-PAAD and GEO-combined datasets were plotted based on the expression profiles of the QYHJ for PAAD-related genes.

Protein-protein interaction network

A protein-protein interaction (PPI) network among QYHJ for PAAD-related genes was constructed using STRING

(PPI Networks Function Enrichment Analysis. Available at: https://string-db.org. Accessed 18 May 2024). Homo sapiens was selected as the annotated species, with a threshold criterion established at a minimum correlation coefficient exceeding 0.400. Cytoscape (version 3.10.2) software was used to construct PPI network. In addition, score was calculated using the degree (Degree Correlation), Maximum Neighborhood Component (MNC), Maximal Clique Centrality (MCC), Edge Percolated Component (EPC) and Closeness Centrality using the CytoHubba plugin. Ultimately, the intersection of the ten most significant genes identified by the algorithms was chosen as hub genes.

Function and pathway enrichment of hub genes

Gene Ontology (GO) and the Kyoto Encyclopedia of Genes and Genomes (KEGG) analyses for hub genes were performed using the ClusterProfiler package (version 4.16.0). The analyses were based on specific selection criteria: p.adjust < 0.05 and p-values corrected by the Benjamini-Hochberg (BH) method.

Prognosis value of hub genes in PAAD

To evaluate the prognostic value of hub genes in PAAD, we performed Cox regression analyses to assess the correlation between hub genes expression and survival status in the TCGA-PAAD dataset. Using the results of the Cox regression analysis, we employed the rms package (version 8.0.0) to create a nomogram that calculated a total score to predict the probability of clinical outcomes. Additionally, the ggDCA package (version 1.1) was used to conduct a decision curve analysis (DCA), which allowed assessment of the model's applicability.

Functional similarity and gene mutation analysis of hub genes

The GOSemSim package (version 2.34.0) was utilized to assess the functional similarity among hub genes. It also computed the geometric means of the functional similarity scores across the biological process (BP), cellular component (CC) and molecular function (MF) categories, producing an overall similarity score. The ggplot2 package (version 3.5.2) was employed to illustrate the functional similarity assessment. Additionally, hub gene mutations in the TCGA-PAAD dataset were analyzed using cBioPortal (cBioPortal for Cancer Genomics. Available at: https://cbioportal.org. Accessed 19 May 2024).

Single sample gene set enrichment analysis (ssGSEA)

The GOSemSim package (version 2.34.0) was utilized to assess the functional similarity among hub genes. It also calculated the geometric means of the functional similarity scores across the biological process (BP), cellular component (CC) and molecular function (MF) categories, producing an overall similarity score. The ggplot2 package (version 3.5.2) was employed to illustrate the functional similarity assessment. Additionally, hub gene mutations in the TCGA-PAAD dataset were analyzed using cBioPortal (cBioPortal for Cancer Genomics. Available at: https://cbioportal.org, Accessed 19 May 2024).

Drug sensitivity analysis

Genomics of Drug Sensitivity in Cancer (GDSC. Available at: https://www.cancerRxgene.org, Accessed 20 May 2024) was used to identify drug response data and genomic markers associated with drug sensitivity in cancer. Specifically, the pRRophetic algorithm was used to calculate the IC50 values based on the TCGA-PAAD dataset to predict sensitivity to anticancer agents, including small-molecule compounds. Subsequently, we compared the differences in drug sensitivity between high-risk and low-risk groups.

Statistical analysis

R software (Version 4.2.2) was used for statistical analyses. To ensure the reproducibility of our results, we fixed the random seed across all randomized operations. To compare the statistical differences between two groups of continuous data with a normal distribution, the t-test was used. For continuous data with non-normal distributions, the Mann-Whitney U test was used to assess differences. Moreover, the Kruskal-Wallis test was used for comparison of differences among more than two groups. Statistical significance among groups with categorical data was analyzed using the Chi-square test or Fisher's exact test. Spearman correlation analysis was performed to calculate correlation coefficients among various molecules. Survival outcomes between the two groups were assessed using Kaplan-Meier curves and log-rank test. Furthermore, the diagnostic potential of hub genes for PAAD was evaluated using Receiver Operating Characteristic (ROC) curves. A p-value less than 0.05 was considered statistically significant.

RESULTS

Screening of QYHJ for PAAD-related genes

The workflow is shown in Fig 1. Seventy active ingredients of QYHJ were identified from the TCMSP database (Table1). Among these compounds, Baihuasheshecao has seven compounds, Banzhilian has twenty-nine, BaiDoukou has twelve, Yiyiren has nine, Jiaogulan has twenty-four and Sheliugu has six. Some compounds are shared by two or more herbs, such as campesterol and rhamnazin, which are shared by Jiaogulan and Banzhilian. Cholestanol (CLR) and sitosterol are shared by Yiyiren, Sheliugu, Jiaogulan and Banzhilian. β-sitosterol is shared by BaiDoukou, Baihuasheshecao and Banzhilian. Luteolin is shared between BaiDoukou and Banzhilian. Quercetin is found in BaiDoukou, Jiaogulan, Baihuasheshecao and Banzhilian. Sheliugu, Yiyiren, Baihuasheshecao and Banzhilian share stigmasterol. Using the TCMSP database, 242 targets related to the active ingredients of QYHJ were obtained and the gene names were transformed using UniProtKB (Table S1). Subsequently, the network of interactions among the targets of the herbal components was constructed using Cytoscape software. (Fig.2A).

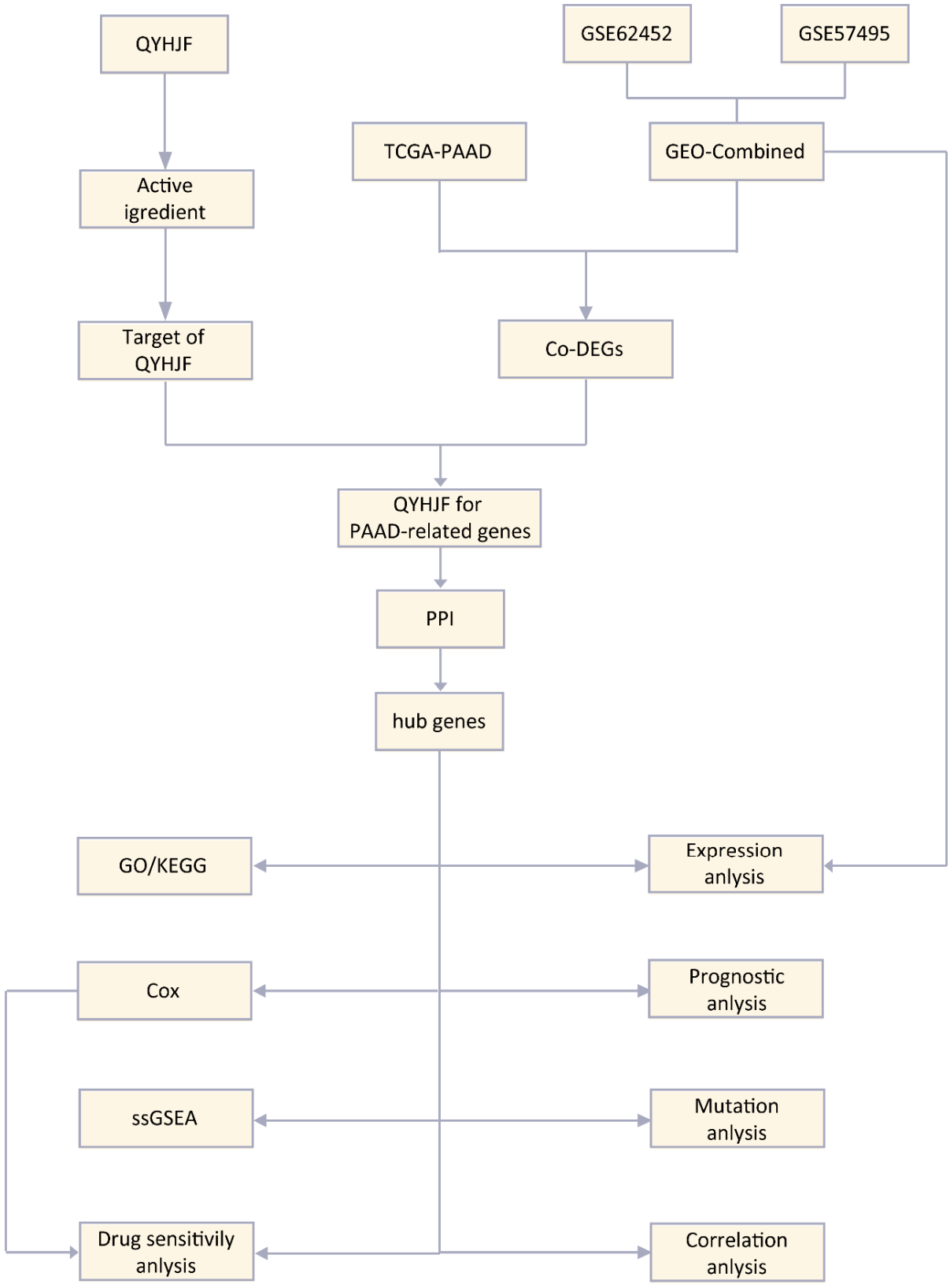

Fig. 1: Flowchart of this study
QYHJ: QingyihuaJi formula; TCGA: The cancer genome atlas; PAAD: Pancreatic adenocarcinoma; GO: Gene ontology; KEGG: Kyoto encyclopedia of genes and genomes; PPI: Protein-protein interaction network.

Table 1: Chemical constituents and ADME parameters of BaiDouKou, SheLiuGu, YiYiRen, JiaoGuLan, BaiHuaSheSheCai, BanZhiLian in QYHJ

NO.	Mol ID	Compound	OB(%)	DL	Herb
BHSSC1	MOL001646	2,3-dimethoxy-6-methyanthraquinone	34.86	0.26	BaiHuaSheSheCao
BHSSC2	MOL001659	Poriferasterol	43.83	0.76	BaiHuaSheSheCao
BHSSC3	MOL001663	(4aS,6aR,6aS,6bR,8aR,10R,12aR,14bS)-10-hydroxy-2,2,6a,6b,9,9,12a-heptamethyl-1,3,4,5,6,6a,7,8,8a,10,11,12,13,14b-tetradecahydropicene-4a-carboxylic acid	32.03	0.76	BaiHuaSheSheCao
BHSSC4	MOL001670	2-methoxy-3-methyl-9,10-anthraquinone	37.83	0.21	BaiHuaSheSheCao
BZL1	MOL001040	(2R)-5,7-dihydroxy-2-(4-hydroxyphenyl)chroman-4-one	42.36	0.21	BanZhiLian
BZL2	MOL012245	5,7,4'-trihydroxy-6-methoxyflavanone	36.63	0.27	BanZhiLian
BZL3	MOL012246	5,7,4'-trihydroxy-8-methoxyflavanone	74.24	0.26	BanZhiLian
BZL4	MOL012248	5-hydroxy-7,8-dimethoxy-2-(4-methoxyphenyl)chromone	65.82	0.33	BanZhiLian
BZL5	MOL012250	7-hydroxy-5,8-dimethoxy-2-phenyl-chromone	43.72	0.25	BanZhiLian
BZL6	MOL012251	Chrysin-5-methylether	37.27	0.2	BanZhiLian
BZL7	MOL012252	9,19-cyclolanost-24-en-3-ol	38.69	0.78	BanZhiLian
BZL8	MOL002776	Baicalin	40.12	0.75	BanZhiLian
BZL9	MOL012266	Rivularin	37.94	0.37	BanZhiLian
BZL10	MOL001973	Sitosteryl acetate	40.39	0.85	BanZhiLian
BZL11	MOL012269	Stigmasta-5,22-dien-3-ol-acetate	46.44	0.86	BanZhiLian
BZL12	MOL012270	Stigmastan-3,5,22-triene	45.03	0.71	BanZhiLian
BZL13	MOL000173	Wogonin	30.68	0.23	BanZhiLian
BZL14	MOL001735	Dinatin	30.97	0.27	BanZhiLian
BZL15	MOL001755	24-Ethylcholest-4-en-3-one	36.08	0.76	BanZhiLian
BZL16	MOL002714	Baicalein	33.52	0.21	BanZhiLian
BZL17	MOL002719	6-Hydroxynaringenin	33.23	0.24	BanZhiLian
BZL18	MOL002915	Salvigenin	49.07	0.33	BanZhiLian
BZL19	MOL005190	Eriodictyol	71.79	0.24	BanZhiLian
BZL20	MOL005869	Daucostero_qt	36.91	0.75	BanZhiLian
BZL21	MOL008206	Moslosooflavone	44.09	0.25	BanZhiLian
BDK1	MOL000224	(4E,6E)-1,7-bis(3,4-dihydroxyphenyl)hepta-4,6-dien-3-one	33.06	0.31	BaiDouKou
BDK2	MOL000228	(2R)-7-hydroxy-5-methoxy-2-phenylchroman-4-one	55.23	0.2	BaiDouKou
BDK3	MOL000230	Pinocembrin	57.56	0.2	BaiDouKou
BDK4	MOL000235	1,7-diphenyl-3,5-dihydroxy-1-heptene	49.01	0.18	BaiDouKou
BDK5	MOL000238	1,7-diphenyl-5-hydroxy-6-hepten-3-one	32.65	0.18	BaiDouKou
BDK6	MOL000239	Jaranol	50.83	0.29	BaiDouKou
BDK7	MOL000242	7-O-Methyleriodictyol	56.56	0.27	BaiDouKou
BDK8	MOL000243	Alpinolide peroxide	87.67	0.19	BaiDouKou
BDK9	MOL000258	Dehydrodiisoeugenol	56.84	0.29	BaiDouKou
BDK10	MOL000260	5-[(2R,3R)-7-methoxy-3-methyl-5-[(E)-prop-1-enyl]-2,3-dihydrobenzofuran-2-yl]-1,3-benzodioxole	65.55	0.4	BaiDouKou
YYR1	MOL001323	Sitosterol alpha1	43.28	0.78	YiYiRen
YYR2	MOL001494	Mandenol	42	0.19	YiYiRen
YYR3	MOL002372	(6Z,10E,14E,18E)-2,6,10,15,19,23-hexamethyltetracosa-2,6,10,14,18,22-hexaene	33.55	0.42	YiYiRen
YYR4	MOL002882	[(2R)-2,3-dihydroxypropyl] (Z)-octadec-9-enoate	34.13	0.3	YiYiRen
YYR5	MOL008118	Coixenolide	32.4	0.43	YiYiRen
YYR6	MOL008121	2-Monoolein	34.23	0.29	YiYiRen

Table 1 is continue……..

NO.	Mol ID	Compound	OB(%)	DL	Herb
JGL1	MOL000338	3'-methyleriodictyol	51.61	0.27	JiaoGuLan
JGL2	MOL004350	Ruvoside_qt	36.12	0.76	JiaoGuLan
JGL3	MOL004355	Spinasterol	42.98	0.76	JiaoGuLan
JGL4	MOL005440	Isofucosterol	43.78	0.76	JiaoGuLan
JGL5	MOL007475	Ginsenoside f2	36.43	0.25	JiaoGuLan
JGL6	MOL009855	(24S)-Ethylcholesta-5,22,25-trans-3beta-ol	46.91	0.76	JiaoGuLan
JGL7	MOL009867	4α,14α-dimethyl-5α-ergosta-7,9(11),24(28)-trien-3β-ol	46.29	0.76	JiaoGuLan
JGL8	MOL009877	Cucurbita-5,24-dienol	44.02	0.74	JiaoGuLan
JGL9	MOL009878	Cyclobuxine	84.48	0.7	JiaoGuLan
JGL10	MOL009888	GypenosideXXXVI_qt	37.85	0.78	JiaoGuLan
JGL11	MOL009928	Gypenoside LXXIV	34.21	0.24	JiaoGuLan
JGL12	MOL009929	Gypenoside LXXIX	37.75	0.25	JiaoGuLan
JGL13	MOL009938	Gypenoside XII	36.43	0.25	JiaoGuLan
JGL14	MOL009943	Gypenoside XL	30.89	0.21	JiaoGuLan
JGL15	MOL009969	GypenosideXXXV_qt	37.73	0.78	JiaoGuLan
JGL16	MOL009971	GypenosideXXVII_qt	30.21	0.74	JiaoGuLan
JGL17	MOL009973	GypenosideXXVIII_qt	32.08	0.74	JiaoGuLan
JGL18	MOL009976	Gypenoside XXXII	34.24	0.25	JiaoGuLan
JGL19	MOL009986	GypentonosideA_qt	36.13	0.8	JiaoGuLan
SLG1	MOL001510	24-epicampesterol	37.58	0.71	SheLiuGu
SLG2	MOL013156	[(2R)-2-[[[(2R)-2-(benzoylamino)-3-phenylpropanoyl]amino]methyl]-3-phenylpropyl] acetate	38.88	0.56	SheLiuGu
(JGL+BZL)1	MOL012254	Campesterol	37.58	0.71	JiaoGuLan+ BanZhiLian
(JGL+BZL)2	MOL000351	Rhamnazin	47.14	0.34	JiaoGuLan+ BanZhiLian
(SLG+YYR+ JGL+BZL)1	MOL000953	CLR	37.87	0.68	SheLiuGu+YiYiRen+ JiaoGuLan+BanZhiLian
(SLG+YYR+ JGL+BZL)2	MOL000359	Sitosterol	36.91	0.75	SheLiuGu+ YiYiRen+JiaoGuLan+ BanZhiLian
BDK+ BHSSC +BZL	MOL000358	Beta-sitosterol	36.91	0.75	BaiDouKou+ BaiHuaSheSheCao +BanZhiLian
BDK+BZL	MOL000006	Luteolin	36.16	0.25	BaiDouKou+ BanZhiLian
BDK+JGL+ BHSSC+BZL	MOL000098	Quercetin	46.43	0.28	BaiDouKou+JiaoGuLan+ BaiHuaSheSheCao+BanZhiLian
SLG+YYR+ BHSSC+BZL	MOL000449	Stigmasterol	43.83	0.76	SheLiuGu+YiYiRen +BaiHuaSheSheCao +BanZhiLian

QYHJ: Qing Yi Hua Ji formula

To explore the targets associated with PAAD, we first performed differential expression analysis on the TCGA-PAAD dataset and the GEO-Combined dataset using the limma package to identify DEGs. In the TCGA-PAAD dataset, 950 genes were upregulated and 5142 genes were downregulated. In the GEO-combined dataset, 3740 genes were upregulated and 4, 440 genes were downregulated.

The DEGs obtained from TCGA-PAAD and GEO-Combined were intersected with the targets of the herbs to identify QYHJ for the PAAD-related genes (Fig.2B). A network plot of the herb-component intersection targets is shown in Fig.2C. QYHJ for PAAD-related genes are listed in Table S2. The volcano plots of the differential expression analysis of TCGA-PAAD and GEO-Combined datasets are shown in Figs. 3A-B and the differences in gene expression of QYHJ for PAAD-related genes in the two datasets are shown in Fig.3C-D.

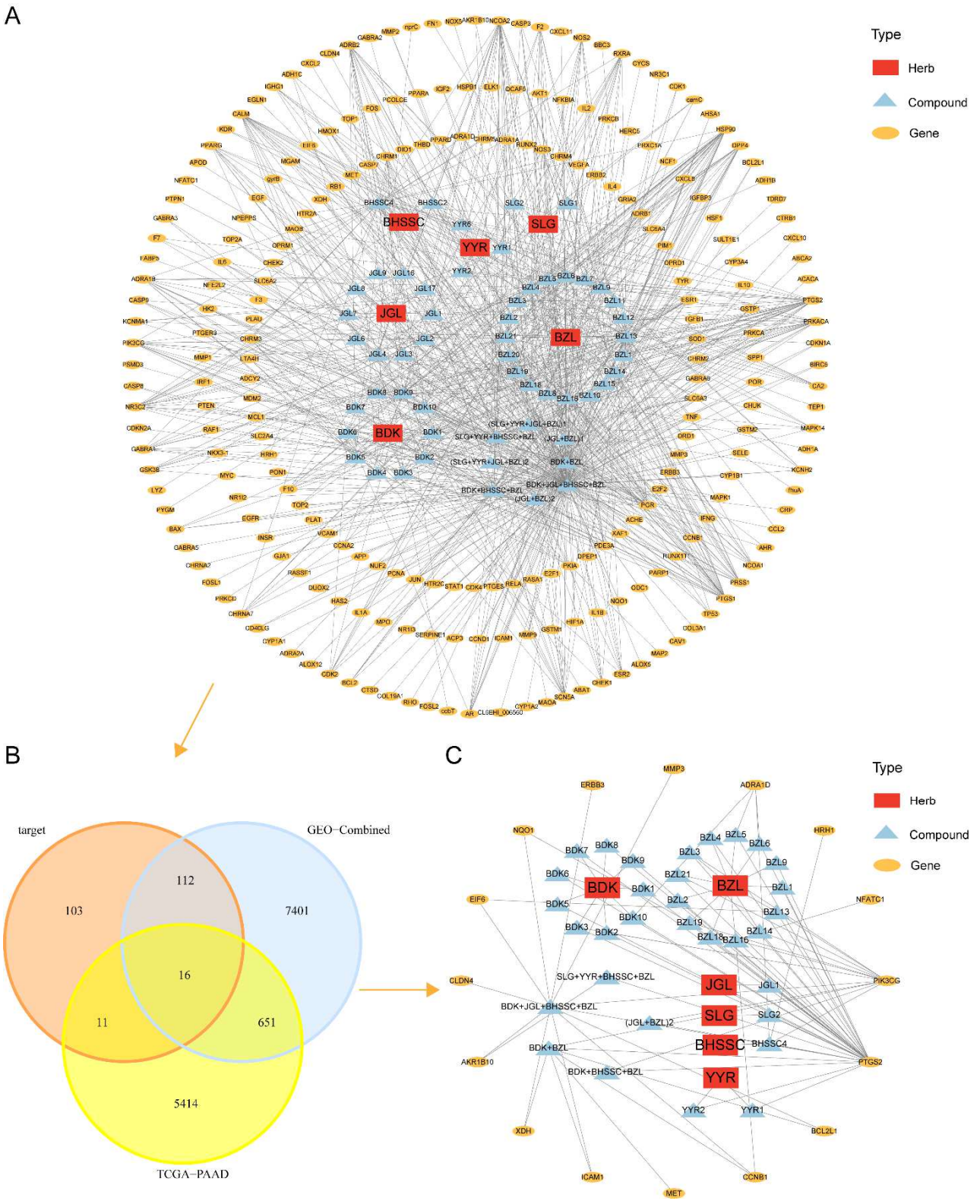

Fig. 2: Screening of QYHJ for PAAD treatment related targets

(A). QYHJ- compound - prediction targets network. (B). TCGA-PAAD-DEGs, GEO-Combined-DEGs and Venn diagram for predicting targets. (C). QYHJ- Component - intersection target interaction network. Yellow ellipses represent targets, blue triangles represent compounds, and red rectangles represent herb. QYHJ: Qing Yi Hua Ji Formula; PAAD: Pancreatic adenocarcinoma; DEGs: Differentially expressed genes.

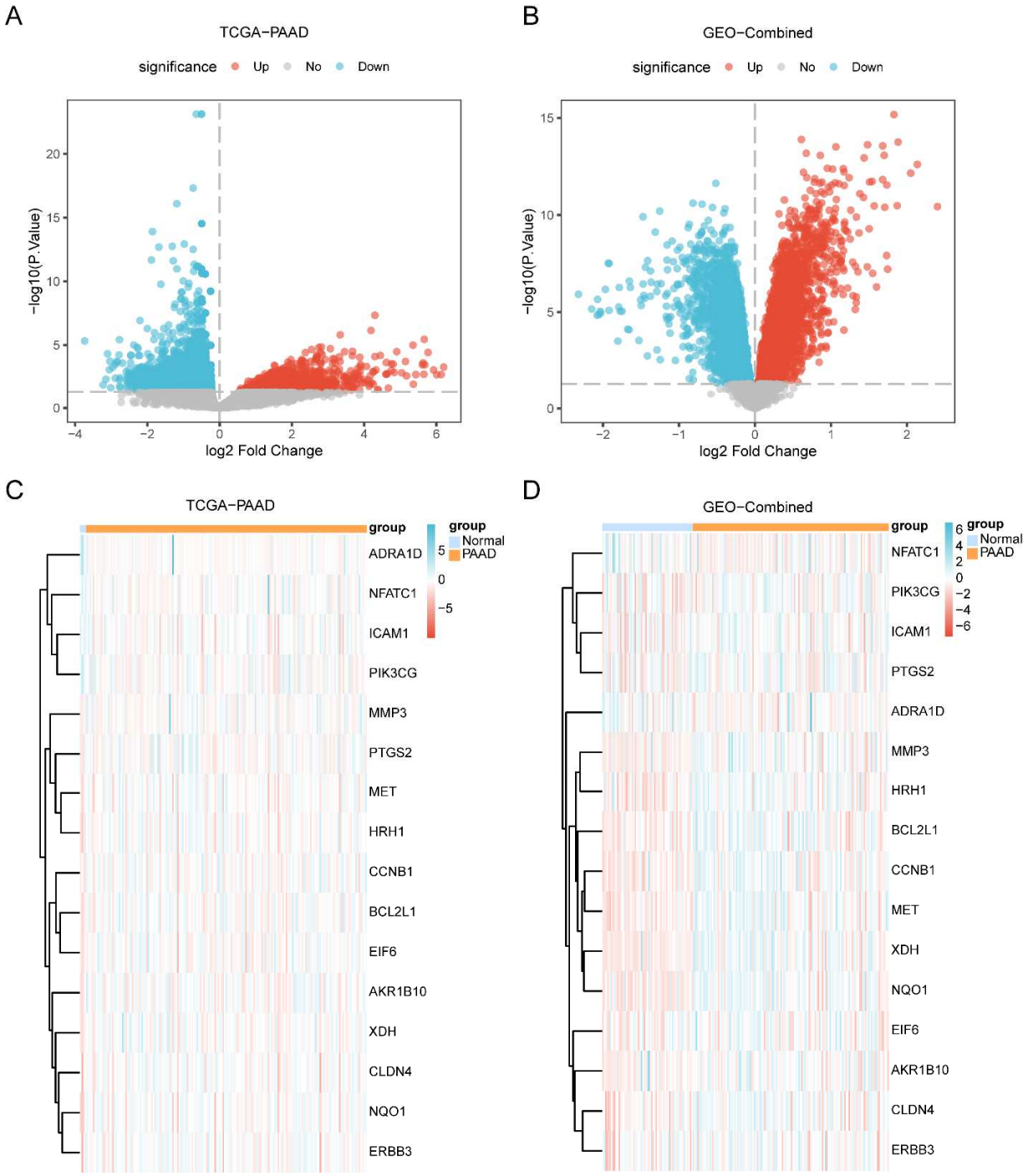

Fig. 3: Differential expression analysis of TCGA-PAAD and GEO-combined datasets

(A). Volcano plot of DEGs between PAAD (n=4) and normal (n=173) tissues in TCGA-PAAD. The Mann-Whitney U test was applied. Red for significantly up-regulated genes, blue for significantly down-regulated genes, and gray for non-significant genes. (B). Volcano plot of DEGs between PAAD (n=132) and normal (n=61) tissues in GEO-combined. The Mann-Whitney U test was applied. Red for significantly up-regulated genes, blue for significantly down-regulated genes, and gray for non-significant genes. (C). Heatmaps of QYHJ for PAAD-related genes of TCGA-PAAD between the PAAD (n=4) and normal (n=173) tissues. Rows represent genes, and columns represent individual patient samples. The color scale represents the Z-score normalized gene expression level, with red indicating expression above the mean and blue indicating expression below the mean. (D). Heatmaps of QYHJ for PAAD-related genes of GEO-combined between the PAAD (n=132) and normal (n=61) tissues. Rows represent genes, and columns represent individual patient samples. The color scale represents the Z-score normalized gene expression level, with red indicating expression above the mean and blue indicating expression below the mean. QYHJ: Qing Yi Hua Ji Formula. PAAD: Pancreatic adenocarcinoma. DEGs: Differentially expressed genes.

Construction of PPI network

The PPI network of the 16 QYHJ for PAAD-related genes was constructed and visualized (Fig.4A). Furthermore, the top 10 gene interaction networks after ranking using the 5 algorithms (MCC, MNC, EPC, Degree and Closeness) were constructed (Fig.4B, Table 2). The hub genes (PTGS2, BCL2L1, ICAM1, MET, NQO1, MMP3, NFATC1, CCNB1 and ERBB3) were identified as those genes that intersected across the five algorithms. (Fig.4C). Among these genes, BCL2L1, PTGS2 and ICAM1 had higher scores for each of the five algorithms (Table 3).

Functional enrichment analysis

We performed GO and KEGG analyses using 9 hub genes: PTGS2, BCL2L1, ICAM1, MET, NQO1, MMP3, NFATC1, CCNB1 and ERBB3. The results of GO analysis (Figs.5A-B) and KEGG analysis (Fig.5C) are presented t. Additionally, we displayed the results of GO analysis (Figs. 5D-E) and KEGG analysis (Fig.5F) as ring network diagrams.

The hub genes exhibited significant enrichment in biological processes (BP), including the cellular response to chemical stress and oxidative stress, as well as the calcineurin-NFAT signaling pathway and its positive regulation (Figs. 5A-C). These genes were mainly enriched in molecular functions (MF) such as antioxidant activity and protein kinase activator activity (Table 4). Additionally, the enrichment of hub genes was observed in signaling pathways associated with NF-κB, TNF, IL-17 and PI3K-Akt (Table 5).

Differential expression and prognostic significance of hub genes

We compared the expression of hub genes (PTGS2, BCL2L1, ICAM1, MET, NQO1, MMP3, NFATC1, CCNB1 and ERBB3) between groups in the TCGA-PAAD (Fig. 6A) and GEO-Combined datasets (Fig. 6B). In the TCGA-PAAD dataset, the expression levels of all hub genes except PTGS2 exhibited a statistically significant difference between the PAAD and normal groups. Similarly, in the GEO-combined dataset, the expression of all hub genes except ERBB3 showed significant differences between the PAAD and control groups.

To further assess the prognostic value of the hub genes, the overall survival (OS) of PAAD patients was analyzed using the Kaplan-Meier (K-M) plot. The expression of six hub genes (BCL2L1, CCNB1, ERBB3, MET, MMP3 and NFATC1) was significantly associated with poor OS (Figs. 6C-H).

Finally, we performed ROC analysis to validate the prognostic value of genes in the TCGA-PAAD and GEO-combined datasets. The results showed that in the TCGA-PAAD dataset, BCL2L1 (AUC=0.824, Fig.7A) CCNB1 (AUC=0.822, Fig.7B), ERBB3 (AUC=0.831, Fig.7C), ICAM1 (AUC=0.857, Fig.7D), MET (AUC=0.831, Fig.7E), MMP3 (AUC=0.834, Fig.7F), NFATC1 (AUC=0.877, Fig.7G) and NQO1 (AUC=0.886, Fig.7H) had diagnostic values for PAAD. Similarly, in the GEO-combined dataset, BCL2L1 (AUC=0.750, Fig.7I), CCNB1 (AUC=0.759, Fig.7J), MET (AUC=0.776, Fig.7L), MMP3 (AUC=0.739, Fig.7M) and NQO1 (AUC=0.786, Fig.7O) had diagnostic value. However, ICAM1 (AUC=0.589, Fig.7K), NFATC1 (AUC=0.636, Fig.7N) and PTGS2 (AUC=0.602, Fig.7P) exhibited low diagnostic value for PAAD.

Cox regression model construction and survival analysis

We performed univariate Cox regression analysis; the results are shown in the forest plot (Fig.8A). The expression of the hub genes was significantly associated with the prognosis of PAAD patients in the TCGA-PAAD dataset ($P< 0.01$).

We then included all the significant variables from the univariate analysis into the multivariate Cox model to obtain the risk score. Next, the patients were divided into high- and low-risk groups according to the risk score. Subsequently, the nomogram was used to evaluate the prognostic significance of the model (Fig.8B). Decision curve analysis (DCA) showed that the predictive value of the model was highest for 5-year outcomes, followed by 3-year and 1-year outcomes (Figs.8C-E).

Functional similarity and mutation analyses

Statistically significant correlations were observed between hub genes in the TCGA-PAAD dataset, with the highest positive correlation between NQO1 and ERBB3 and the highest negative correlation between NFATC1 and ERBB3 (Fig. 9A). Furthermore, functional similarity analysis revealed that ERBB3 had the greatest functional significance (Fig. 9B).

Mutation status analysis revealed that missense and nonsense mutations were the main types in hub genes of the TCGA-PAAD dataset, with missense mutations being predominant (Fig.9C). Moreover, single nucleotide variants (SNVs), particularly C > T, were the most frequent mutation types observed, followed by C > A.

Immune Infiltration analysis with ssGSEA

Immune cell infiltration abundance in the two groups is shown in Fig. 10A. Nine immune cells showed significant differences between the two groups ($P < 0.05$, Fig. 10B). The correlation between these nine immune cells and hub genes (PTGS2, BCL2L, ICAM1, MET, NQO1, MMP3, NFATC1, CCNB1 and ERBB3) is shown in a heatmap (Fig. 10C). The results indicate that ICAM1, MET, NQO1 and ERBB3 are positively associated with T helper 2 (Th2) and T helper 17 (Th17) cells.

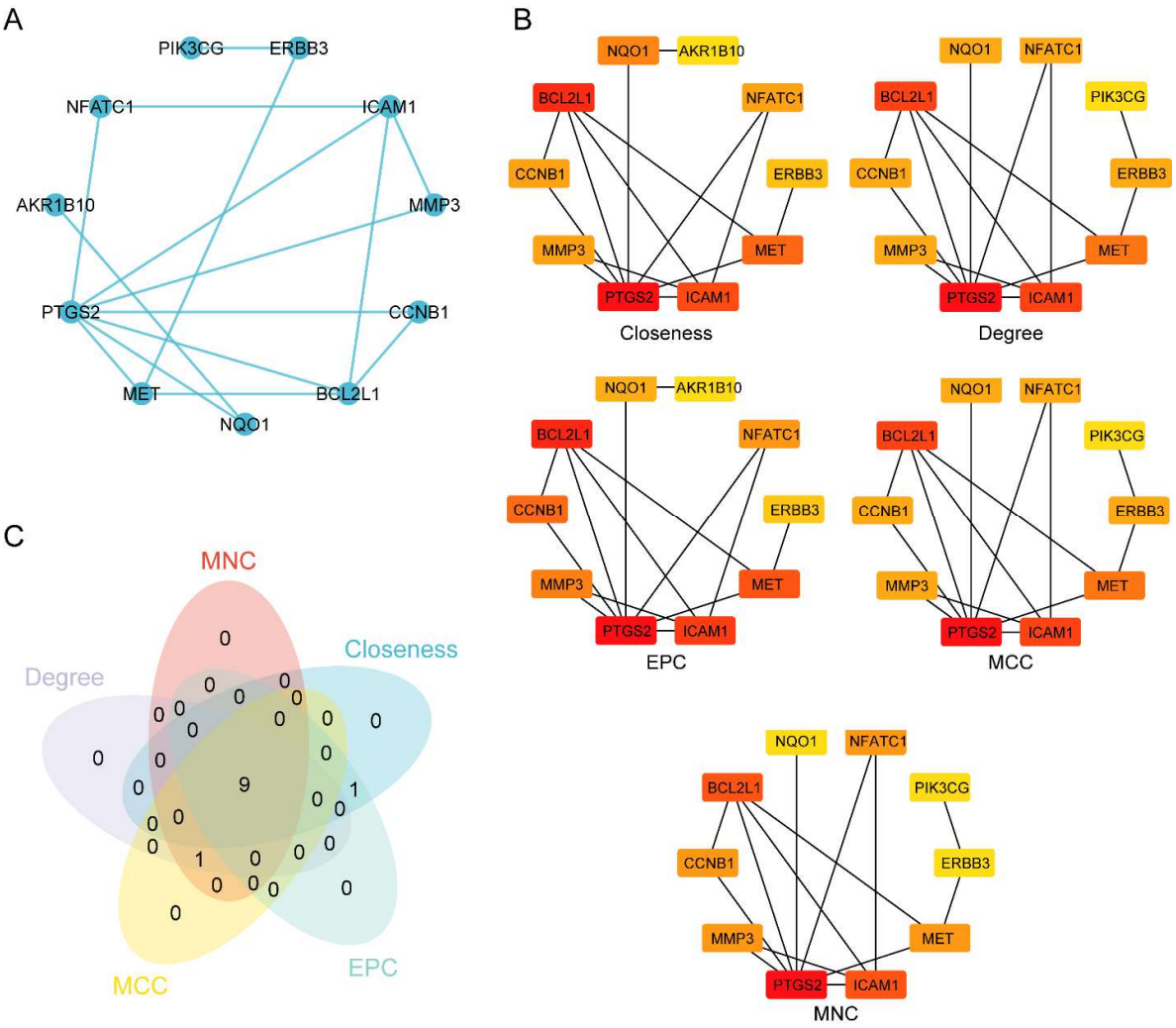

Fig. 4: Protein-protein interaction network

(A). PPI network of QYHJF for PAAD-related genes. The network was constructed by importing the list of 16 PAAD-related genes into the STRING database and retrieving interactions with a combined confidence score > 0.4. The resulting network was visualized in Cytoscape (v3.10.2). (B). Comparative analysis of top 10 hub genes identified by five (Closeness, Degree, EPC, MCC and MNC) ranking algorithms in cytoHubba. The color intensity of nodes represents the score. (C). Venn diagram illustrating the overlap of the top 10 hub genes identified by the five algorithms. QYHJ: Qing Yi Hua Ji Formula; PAAD: Pancreatic adenocarcinoma; PPI Network: protein-protein interaction. Degree: Degree correlation; MNC: Maximum neighborhood component; MCC: Maximal clique centrality; EPC: Edge percolated component; Closeness: Closeness centrality.

Table 2: Calculation results of five cytoHubba algorithms.

Closeness	Degree	EPC	MCC	MNC
PTGS2	PTGS2	PTGS2	PTGS2	PTGS2
BCL2L1	BCL2L1	BCL2L1	BCL2L1	BCL2L1
ICAM1	ICAM1	ICAM1	ICAM1	ICAM1
MET	MET	MET	MET	MET
NQO1	ERBB3	CCNB1	ERBB3	MMP3
MMP3	MMP3	MMP3	MMP3	NFATC1
NFATC1	NQO1	NFATC1	NQO1	CCNB1
CCNB1	NFATC1	NQO1	NFATC1	PIK3CG
ERBB3	CCNB1	ERBB3	CCNB1	ERBB3
AKR1B10	PIK3CG	AKR1B10	PIK3CG	NQO1

Degree: Degree Correlation; MNC: Maximum Neighborhood Component; MCC: Maximal Clique Centrality; EPC: Edge Percolated Component; Closeness: Closeness Centrality

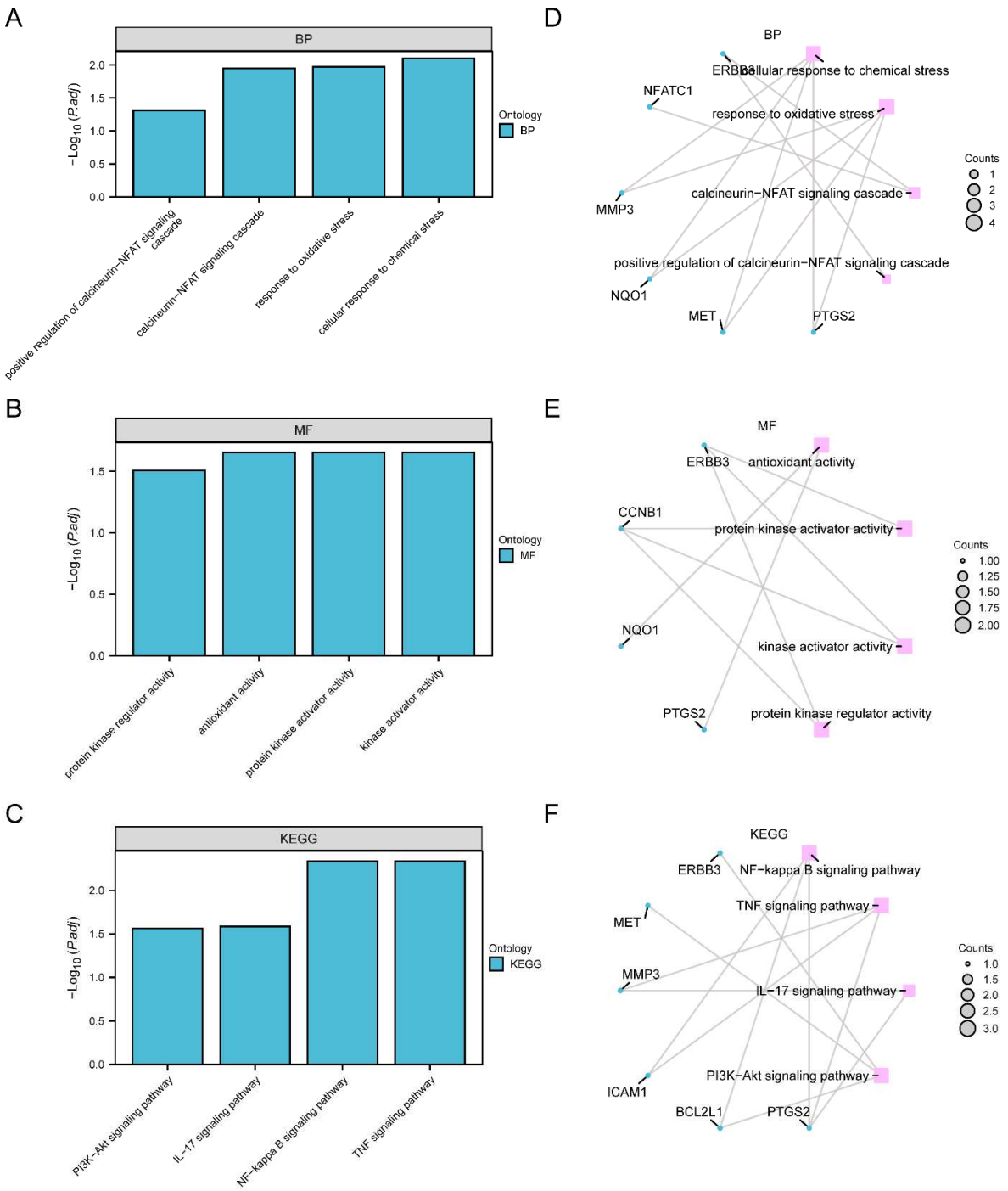

Fig. 5: GO and KEGG enrichment analysis of hub genes

(A-B). GO enrichment analysis of the identified hub genes. Bar plot displaying the top 8 significantly enriched GO terms (BP, A) and (MF, B) for the 9 hub genes. Enrichment analysis was performed using the clusterProfiler R package (v4.16.0). Only terms with an adjusted p-value < 0.05 are shown. (C). KEGG pathway enrichment analysis of the identified hub genes. Bar plot showing the top 10 significantly enriched KEGG pathways for the 9 hub genes. Enrichment analysis was performed using the clusterProfiler R package (v4.16.0). Only terms with an adjusted p-value < 0.05 are shown. (D-E). Circular network plot of GO enrichment analysis for hub genes. The circular visualization summarizes the top 8 significantly enriched GO terms from GO categories: BP (D) and MF (E). Enrichment analysis was conducted using the clusterProfiler R package (v4.16.0). Significantly enriched terms were filtered by an adjusted P-value < 0.05. (F). Circular network plot of KEGG enrichment analysis of hub genes. This circular layout presents both the significance of the enriched KEGG pathways and the interactions between them based on hub genes. Enrichment analysis was conducted using the clusterProfiler R package (v4.16.0) against the KEGG database. Significance was defined as an Adjusted P-value < 0.05. GO: Gene Ontology. BP: Biological process. MF: Molecular function. KEGG: Kyoto encyclopedia of genes and genomes

Table 3: Topological parameters of hub genes

	Closeness	Degree	EPC	MCC	MNC
PTGS2	8.333333	7	5.478	11	6
BCL2L1	6.666667	4	4.838	6	4
ICAM1	6.416667	4	4.832	6	4
MET	6.333333	3	4.415	3	2
NQO1	5.583333	2	3.56	2	1
MMP3	5.416667	2	4.003	2	2
NFATC1	5.416667	2	3.99	2	2
CCNB1	5.416667	2	4.017	2	2
ERBB3	4.916667	2	2.863	2	1

Table 4: GO analysis results

Ontology	ID	Description	Gene ratio	Bg ratio	*p-value*	p.adjust	*q-value*
BP	GO:0062197	cellular response to chemical stress	4/9	332/18800	1.12E-05	0.007945	0.003532
BP	GO:0006979	response to oxidative stress	4/9	433/18800	3.19E-05	0.010648	0.004734
BP	GO:0033173	calcineurin-NFAT signaling cascade	2/9	44/18800	0.000191	0.011253	0.005002
BP	GO:0070886	positive regulation of calcineurin-NFAT signaling cascade	1/9	16/18800	0.007635	0.048664	0.021633
MF	GO:0016209	antioxidant activity	2/9	85/18410	0.000743	0.022306	0.009131
MF	GO:0030295	protein kinase activator activity	2/9	104/18410	0.001109	0.022306	0.009131
MF	GO:0019209	kinase activator activity	2/9	110/18410	0.001239	0.022306	0.009131
MF	GO:0019887	protein kinase regulator activity	2/9	207/18410	0.0043	0.031117	0.012738

GO: Gene Ontology; BP: biological process; MF: molecular function

Table 5: KEGG analysis results

Ontology	ID	Description	Gene ratio	Bg ratio	*p-value*	p.adjust	*q-value*
BP	GO:0062197	cellular response to chemical stress	4/9	332/18800	1.12E-05	0.007945	0.003532
BP	GO:0006979	response to oxidative stress	4/9	433/18800	3.19E-05	0.010648	0.004734
BP	GO:0033173	calcineurin-NFAT signaling cascade	2/9	44/18800	0.000191	0.011253	0.005002
BP	GO:0070886	positive regulation of calcineurin-NFAT signaling cascade	1/9	16/18800	0.007635	0.048664	0.021633
MF	GO:0016209	antioxidant activity	2/9	85/18410	0.000743	0.022306	0.009131
MF	GO:0030295	protein kinase activator activity	2/9	104/18410	0.001109	0.022306	0.009131
MF	GO:0019209	kinase activator activity	2/9	110/18410	0.001239	0.022306	0.009131
MF	GO:0019887	protein kinase regulator activity	2/9	207/18410	0.0043	0.031117	0.012738
KEGG	hsa04064	NF-kappa B signaling pathway	3/9	104/8164	0.00016	0.004623	0.003244
KEGG	hsa04668	TNF signaling pathway	3/9	112/8164	0.000199	0.004623	0.003244
KEGG	hsa04657	IL-17 signaling pathway	2/9	94/8164	0.00448	0.026041	0.018274
KEGG	hsa04151	PI3K-Akt signaling pathway	3/9	354/8164	0.005586	0.02734	0.019186

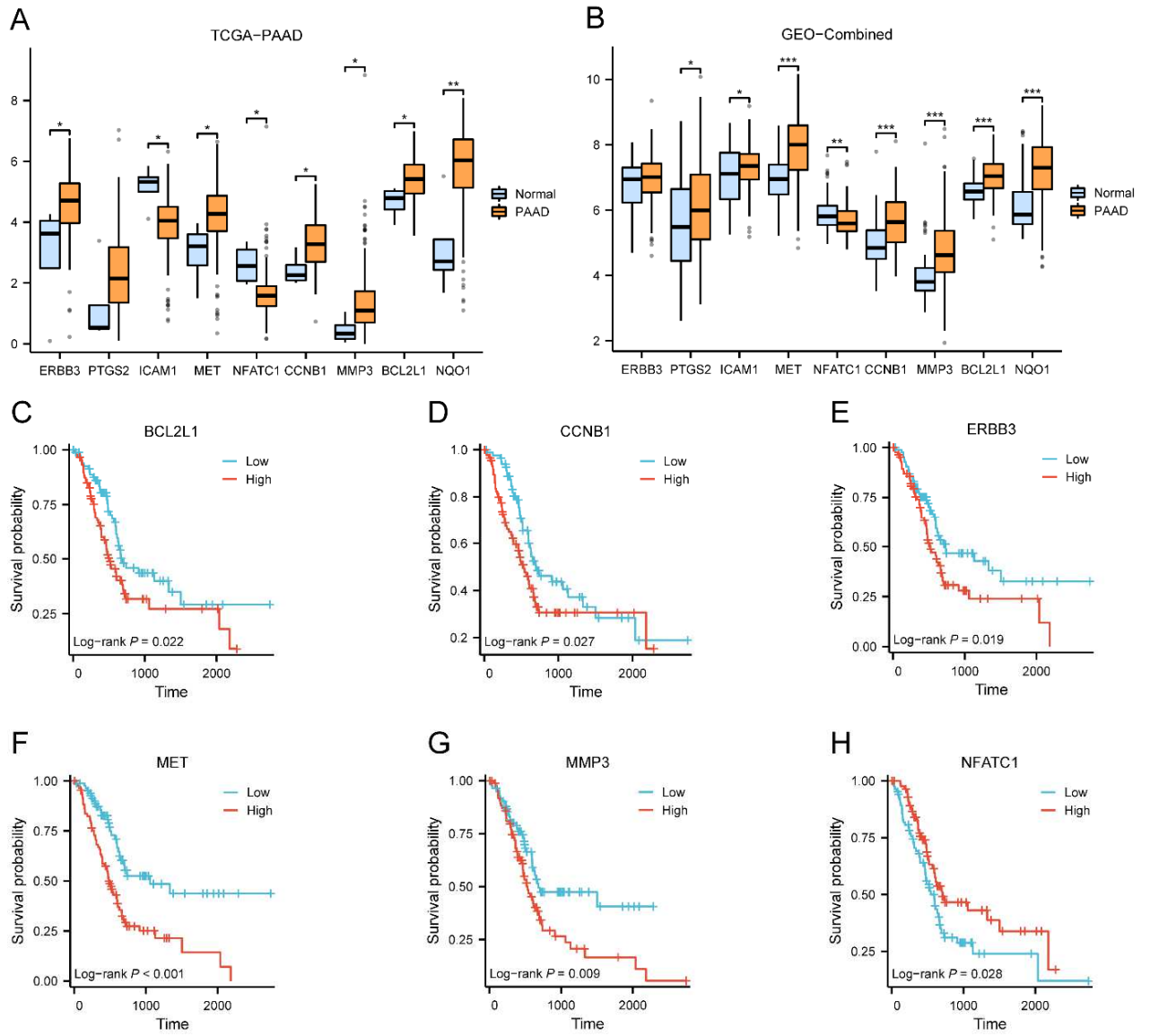

Fig. 6: Differential expression and prognosis analysis of hub genes in PAAD and normal groups
(A). Expression of hub genes in the TCGA-PAAD dataset between PAAD (n=173) and normal (n=4) groups. (B). Expression of hub genes in the GEO-combined dataset between the PAAD (n=132) and the normal (n=61) groups. (C-H). KM plotters of six hub genes in the TCGA-PAAD dataset (n=173). PAAD: Pancreatic adenocarcinoma; OS: Overall survival; KM: Kaplan-Meier. (* P < 0.05; ** P < 0.01; *** P < 0.001).

Drug susceptibility prediction

The sensitivity to common anticancer drugs in high- and low-risk groups was predicted using data from the GDSC. First, we evaluated the differences in drug sensitivity between the two groups. We then compared the sensitivity of the top 20 drugs (EHT-1864, Temsirolimus, NU7441, AZD2281, AMG706, Nutlin-3a, Axitinib, PD-0332991, CEP-701, NVP-BEZ235, PD-173074, GDC-0449, AG-014699, AZD8055, ZM-447439, Metformin, Vorinostat, CCT007093, TW-37, ATRA) that exhibited the largest differences in sensitivity between the two groups (Figs. 11A–T). Among the 20 drugs with significant differences, we observed that the IC50 values were higher in the high-risk cohort than in the low-risk cohort. This indicates that individuals in the low-risk group are more sensitive to these drugs.

DISCUSSION

Chemotherapy is currently the main treatment for PAAD; however, most drugs show limited efficacy and cause severe adverse reactions. TCM can not only prolong the survival time of PAAD patients but also plays a crucial role in improving quality of life (Shi *et al*., 2018; Zhang *et al*., 2020). TCM and its compounds involve a complex interplay of multiple bioactive components; therefore, investigating the underlying mechanisms of its action is crucial.

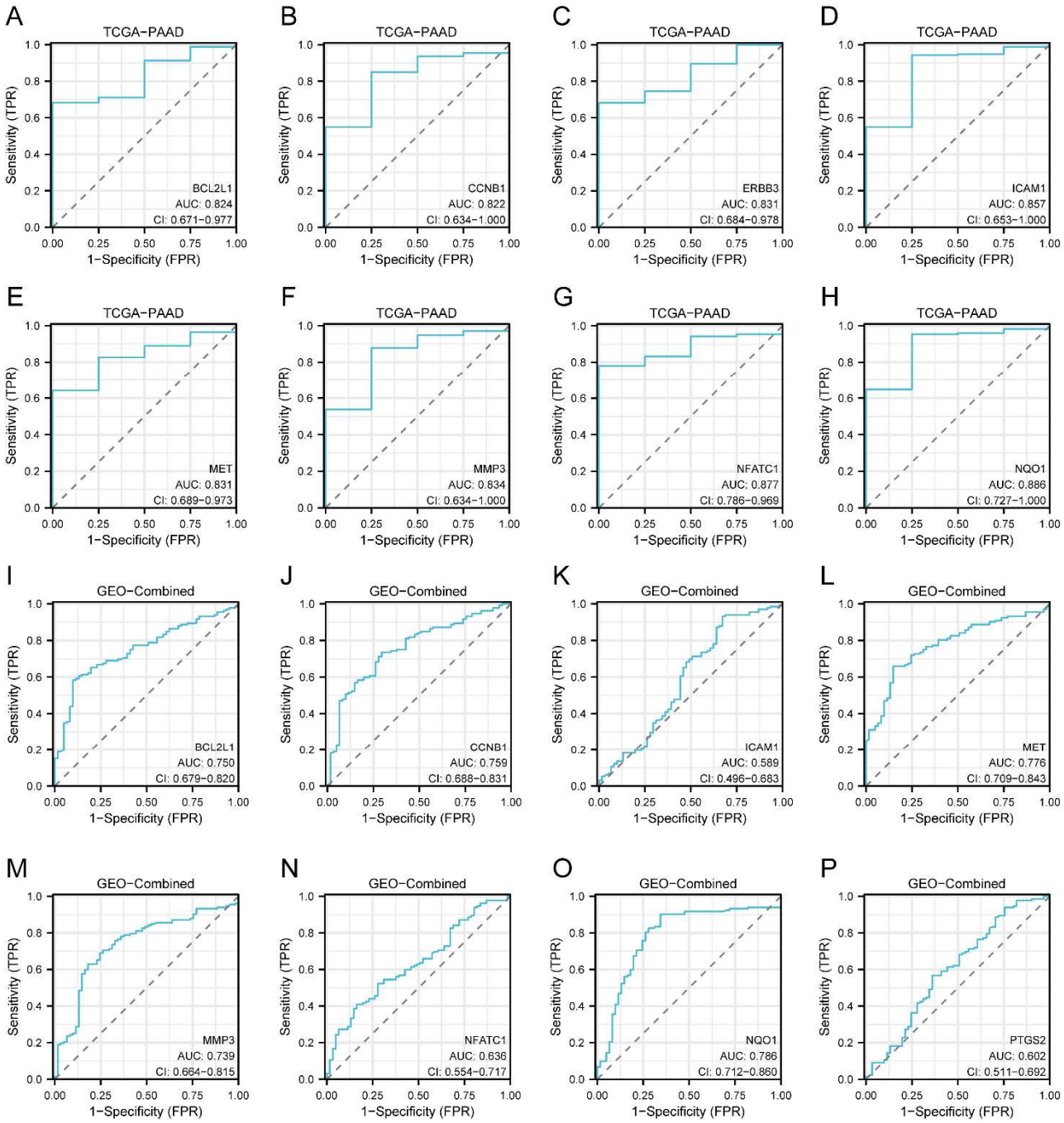

Fig. 7: ROC curve of hub genes in PAAD and normal groups
(A-H). ROC curve of each hub genes in the TCGA-PAAD dataset (PAAD n=173, normal n=4) (I-P). ROC curve of each hub genes in the GEO-Combined datasets (PAAD n=132, normal n=61) PAAD: Pancreatic adenocarcinoma; ROC: receiver operating characteristic curve; AUC: Area under curve.

QYHJ was developed based on the concept of “dampness and heat accumulation” in PAAD, with the main treatment principle being “clearing heat and drying dampness.” It has been used for comprehensive treatment of PAAD patients (Chen *et al*., 2019; Shi *et al*., 2025). However, the main targets and mechanisms through which QYHJ treats PAAD remain unclear.

Network pharmacology is an interconnected framework based on the principle of "disease-gene-target-medicine". It systematically and scientifically evaluates how intervention drugs affect the disease network to reveal their mechanisms of action. Thus, in this study, an integrative analysis of network pharmacology and bioinformatics was performed to explore hub genes with QYHJ for PAAD treatment and its potential clinical significance.

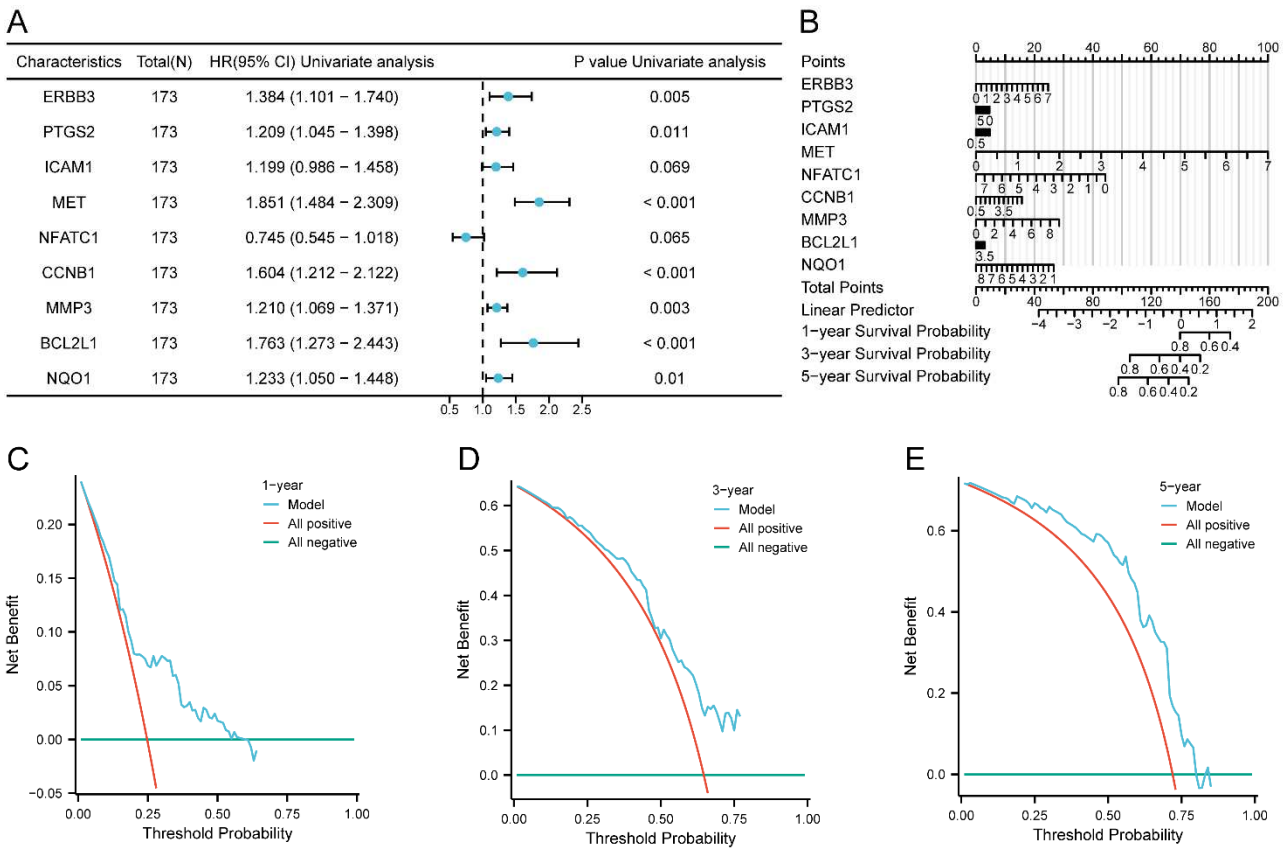

Fig. 8: Cox regression model construction and prognostic value of hub genes

(A). Forest plot of multivariate Cox regression analysis for hub genes in the TCGA-PAAD dataset (n=173). This forest plot displays the results of the multivariate Cox proportional hazards regression analysis for the association between the expression levels of the hub genes and overall survival (OS). P-values were derived from the Wald test, and a P-value < 0.05 was considered statistically significant. (B). Prognostic nomogram for predicting 1-, 3- and 5-year overall survival from patients in the TCGA-PAAD dataset (n=173). For an individual patient, values for each parameter are projected upward to the 'Points' line to obtain a partial score. The sum of these partial scores yields the 'Total Points', which is then projected downward to the bottom axes to estimate the probability of survival at 1, 3 and 5 years. C-E. DCA plots at 1 year (C), 3 years (D), and 5 years (E) of prognostic model in the TCGA-PAAD dataset (n=173). Decision curve analysis evaluating the clinical utility of prognostic models. The y-axis represents the net benefit, which incorporates the trade-off between true positives (benefits) and false positives (harms). The x-axis represents the threshold probability, which is the minimum probability of death at which a patient or clinician would opt for intervention. PAAD: Pancreatic adenocarcinoma; DCA: Decision curve analysis.

Currently, we established a network comprising "QYHJ target genes-PAAD DEGs" and identified 16 PAAD-related genes involved in QYHJ treatment. Furthermore, a PPI network was constructed to identify nine hub genes (PTGS2, BCL2L1, ICAM1, MET, NQO1, MMP3, NFATC1, CCNB1 and ERBB3) related to QYHJ. Some hub genes, such as ICAM1, MET and NQO1, were reported in previous studies (Qian *et al*., 2020; Yang *et al*., 2022). Others were only found in our study and require further investigation.

ICAM1 is an inflammation-related gene that promotes PAAD metastasis. It also contributes to poor prognosis in PAAD patients. Another study showed that QYHJ decreased ICAM1 expression and exerted an inhibitory effect on PAAD (Yang *et al*., 2022). BCL2L1 encodes a critical anti-apoptotic protein that promotes PAAD cell survival. QYHJ suppresses PAAD growth and progression through the BCL2/Bax pathway (Yang *et al*., 2022). Similarly, the expression level of MET was significantly elevated and associated with unfavorable survival outcomes in PAAD (Lux *et al*., 2019; Zhou *et al*., 2019). Overall, our findings align with previous studies, suggesting that QYHJ has the potential to mitigate inflammation and promote apoptosis in PAAD. Recent investigations have indicated a strong correlation between CCNB1 and the progression of PAAD, suggesting that it may serve as a promising biomarker and therapeutic target for the treatment of this malignancy (Zeng and Fan, 2022). Meanwhile, ERBB3 expression is upregulated in PAAD and is correlated with the clinical stage and poor overall survival of PAAD (Liu *et al*., 2021).The ERBB3 pathway is involved in cancer stem cells (CSCs) generation and the inhibition of ERBB3 can suppress PAAD cell proliferation and tumorigenicity (Hassan *et al*., 2022). In addition, over-expression of MMP3 promoted PAAD invasion and

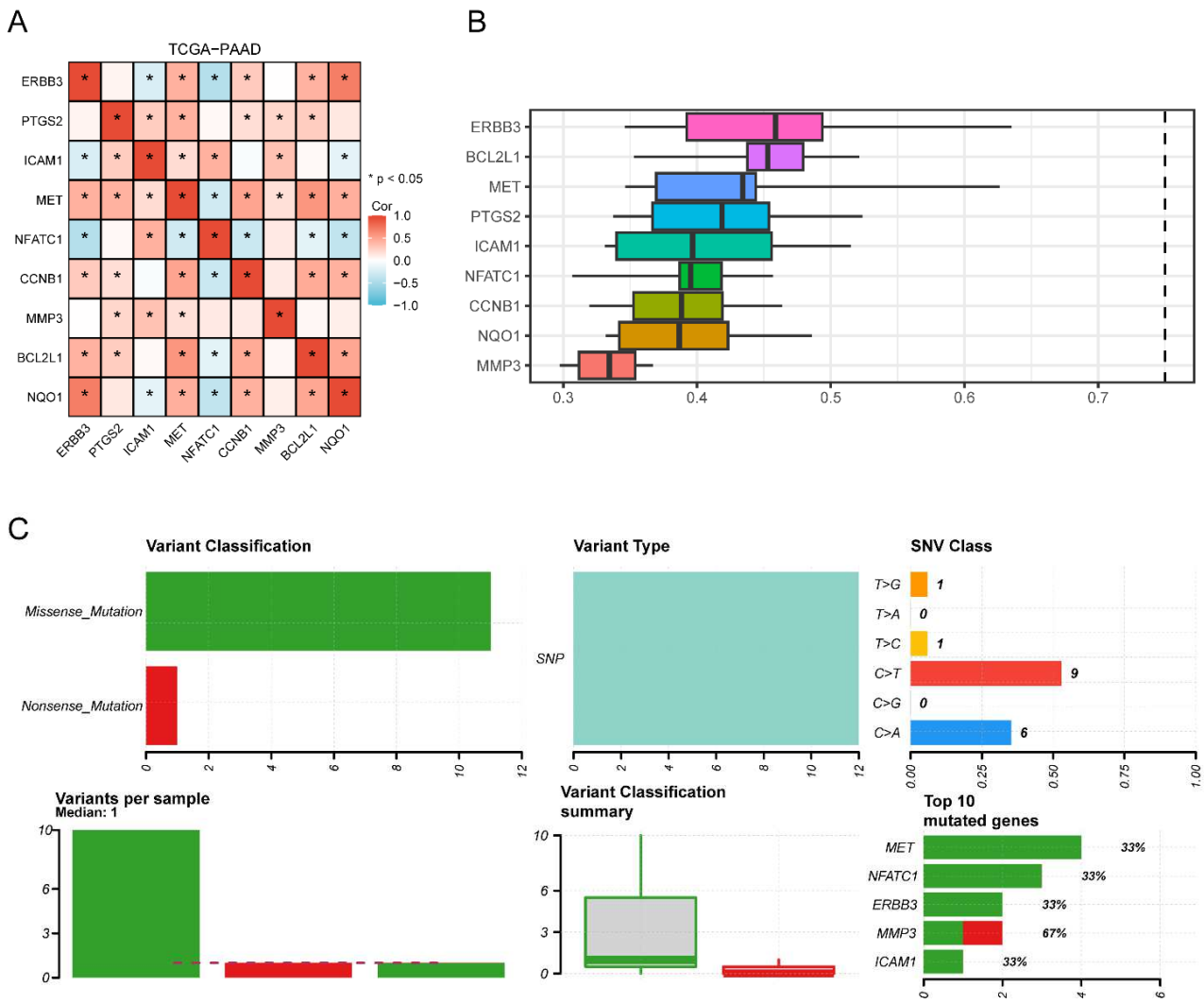

Fig. 9: Gene correlation, functional similarity and gene mutation analysis of hub genes
(A). Correlation analysis of the hub gene in TCGA-PAAD dataset. Heatmap depicting the pairwise Pearson correlation of expression levels among the nine hub genes. The color intensity and the number within each cell represent the Pearson correlation coefficient (r), ranging from -1 (strong negative correlation, blue) to +1 (strong positive correlation, red). Asterisks indicate the statistical significance of the correlation (*P < 0.05). (B). Functional similarity analysis of the hub genes. Boxplot comparing the functional similarity scores between the hub genes. In the boxplots, the central line indicates the median, the box limits represent the upper and lower quartiles (25th and 75th percentiles), and the whiskers extend to 1.5 times the interquartile range (IQR). (C). Mutational landscape of hub genes in TCGA-PAAD dataset. Somatic variants were analyzed and visualized using the maftools R package (v2.24.0). The predominant mutation type is Missense Mutation. SNPs are the primary mutation type observed in the hub genes. SNP: Single nucleotide polymorphisms; PAAD: Pancreatic adenocarcinoma.

metastasis and inhibition of MMP-3 expression has been shown to impede the development of resistance to gemcitabine and to hinder PAAD progression (Deng *et al*., 2022).

Inhibiting MMP3 activity could attenuate the metastasis of PAAD, suggesting that MMP-3 may be a promising therapeutic target for PC (Sayed *et al*., 2022; Zhang *et al*., 2023). The results of this study indicate that low NFATC1 expression is closely associated with poor prognosis in PAAD patients. This conclusion differs from some previous reports, which suggested that high NFATC1 expression correlates with an unfavorable prognosis in PAAD (Chen *et al*., 2015; Chen *et al*., 2017). The discrepancy may be attributed to differences in study populations, sample sizes, detection methods, grouping criteria and cohort heterogeneity. Data and survival analysis from this cohort support the notion that patients with low NFATC1 expression exhibit higher clinical risk, suggesting that NFATC1 may exert differential regulatory roles across different populations or tumor subtypes. The specific mechanisms underlying this observation require further elucidation. Future studies involving larger sample

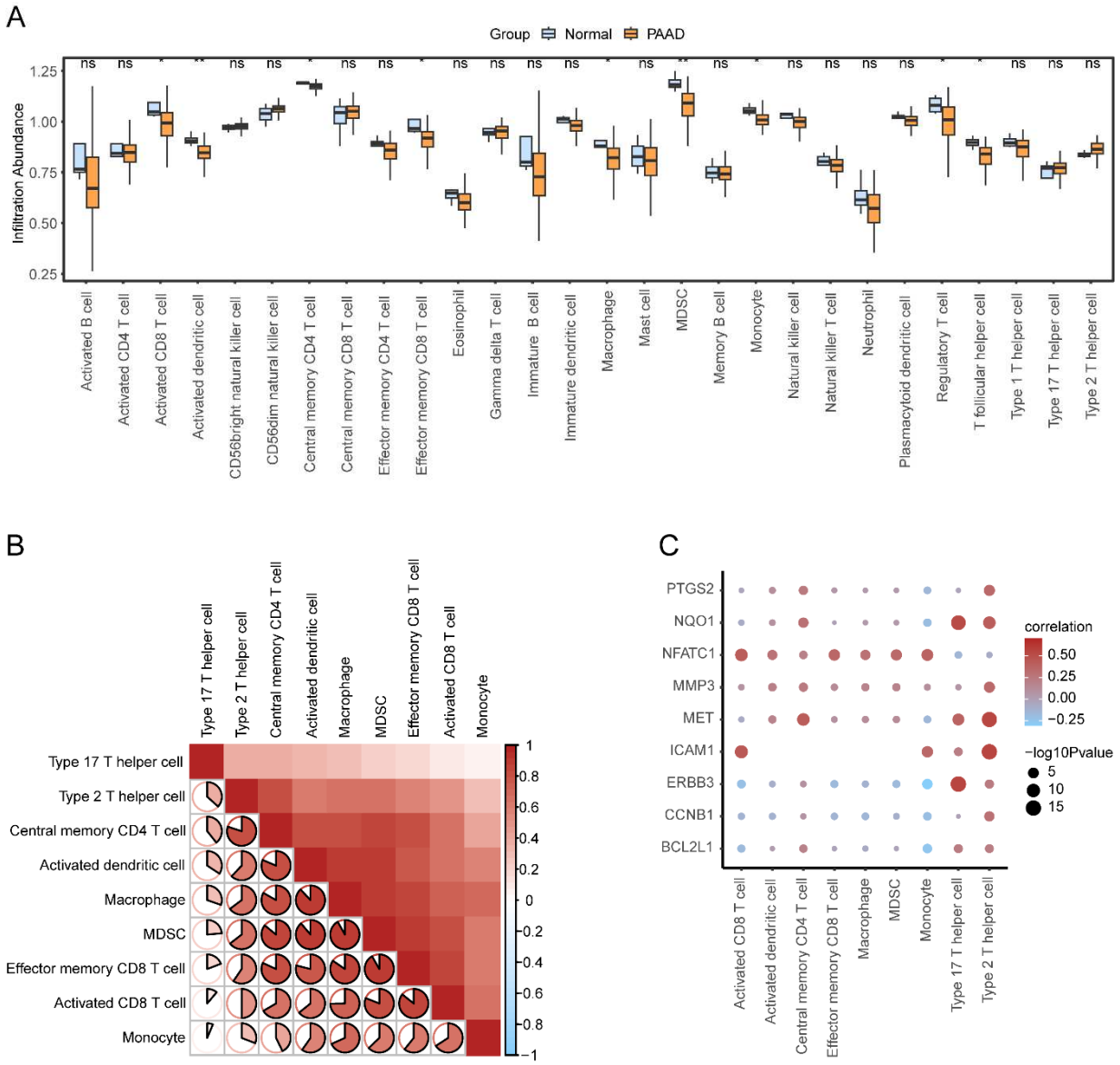

Fig. 10: Analysis of immune infiltration

(A). Comparison of immune cell infiltration levels between the PAAD and normal groups in TCGA-PAAD dataset. Statistical significance was determined by the Wilcoxon rank-sum test. (*P < 0.05, **P < 0.01); (B). Correlation analysis between the nine immune cells. Heatmap of pairwise correlations between the abundance of nine immune cell types in the TCGA-PAAD dataset. The color key represents the Spearman correlation coefficient (r), ranging from -1 (perfect negative correlation, blue) to +1 (perfect positive correlation, red); (C). Correlations between the expression levels of hub genes and the infiltration abundance of 9 immune cells. Spearman correlation heatmap illustrating the relationships between the expression of 9 hub genes and the relative abundance of 9 key immune cell types in the TCGA-PAAD dataset. The color intensity and the number in each tile correspond to the Spearman's rho value. Rows (genes) and columns (immune cells) are ordered by hierarchical clustering based on their correlation profiles.

sizes and multi-center cohorts are warranted to validate the prognostic value and molecular mechanisms of NFATC1. Besides, inhibiting PTGS2 can alleviate malignant tumor phenotypes of PAAD cells (Jiao *et al*., 2022). Collectively, these hub genes are important in the development and progression of PAAD and warrant further investigation.

GO analysis revealed that the hub genes relate to several biological processes, including cell proliferation, migration, tumor microenvironment and immunogenicity. In this study, QYHJ acted on PAAD via various biological pathways. KEGG analysis showed that the hub genes are involved in the PI3K/AKT, IL-17, NF-kappa B and TNF signaling pathways, suggesting a potential mechanism for PAAD progression. The PI3K/AKT pathway, recognized as important in PAAD, was also identified in this study. Studies have demonstrated that QYHJ suppresses the progression of PAAD via modulating the PI3K/AKT/mTOR pathway (Qian *et al*., 2023; Yang *et al*., 2022).

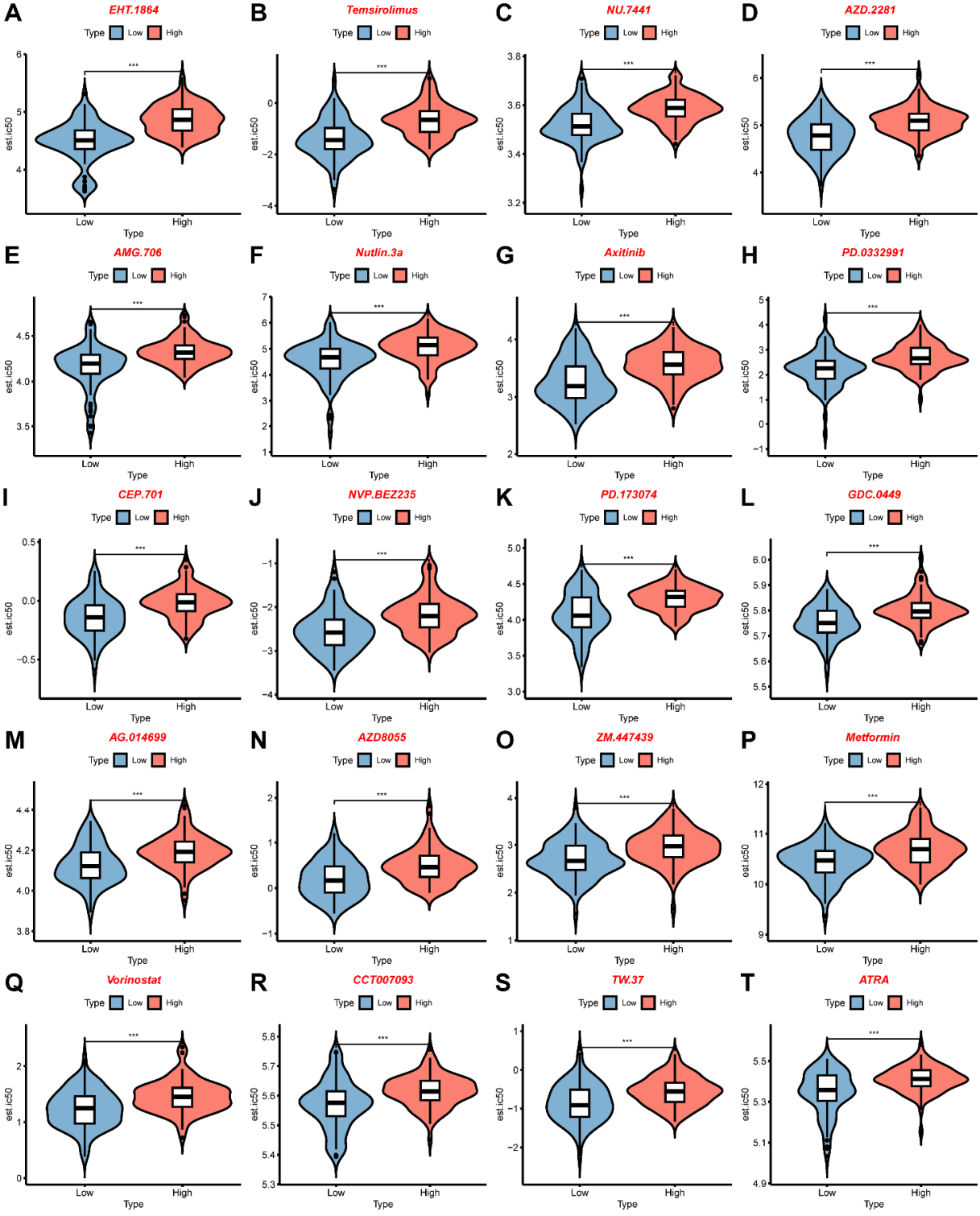

Fig. 11: Drug susceptibility analysis

(A-T). Comparison of drug sensitivity between high and low risk scores groups in the TCGA-PAAD dataset. Drugs: EHT.1864 (A), Temsirolimus (B), NU.7441 (C), AZD.2281 (D), AMG.706 (E), Nutlin.3a (F), Axitinib (G), PD.0332991 (H), CEP.701 (I), NVP.BEZ235 (J), PD.173074 (K), GDC.0449 (L), AG.014699 (M), AZD8055 (N), ZM.447439 (O), Metformin (P), Vorinostat (Q), CCT007093 (R), TW.37 (S), ATRA (T). Violin plots overlaid with box plots showing the distribution of half-maximal inhibitory concentration (IC_{50}) values for drug in high-risk (n =) and low-risk (n =) groups. Lower IC_{50} values indicate higher drug sensitivity. The center line represents the median, the box indicates the interquartile range (IQR) and the whiskers extend to 1.5× IQR. The p-value was calculated using a two-sided Mann-Whitney U test. (*** $P < 0.001$).

These data suggested that the PI3K/AKT/mTOR pathway is crucial in PAAD progression and therapy using TCM. However, the roles of the other three pathways in PAAD require further investigation.

Furthermore, ROC analyses showed that the AUC values of BCL2L1, CCNB1, MET, MMP3 and NQO1 were all greater than 0.7 in these two datasets. This indicates that these hub genes could serve as potential diagnostic markers for PAAD. Since MET and NQO1 have been reported to be positively correlated with TNM stage (Qian *et al*., 2020). We performed survival analysis and found that five genes (BCL2L1, CCNB1, ERBB3, MET and MMP3) were highly expressed and associated with poor prognosis. These results align with the earlier studies reporting the prognostic value of CCNB1 and ERBB3 in PAAD (Liu *et al*., 2021; Zhou *et al*., 2018). The diagnostic efficacy of some genes (NQO1/ICAM1) varied between the two datasets, mainly due to uneven sample sizes, different sequencing platforms and data source heterogeneity. Additionally, the nomogram constructed using the hub genes demonstrated good predictive ability for prognosis, suggesting that these genes may serve as biomarkers for prognosis prediction in patients with PAAD. It should be noted that the AUC values of some genes show inconsistencies across different datasets. TCGA-PAAD includes a few normal samples, which may lead to overestimation of AUC and reduced stability. In contrast, GEO combined data have larger sample sizes, resulting in more robust findings. Additionally, differences in platforms (high-throughput sequencing versus microarrays) and data source heterogeneity (different centers and processing procedures) can affect expression profiles and diagnostic performance. Therefore, the current results are preliminary and require further validation in independent, multi-center cohorts with larger sample sizes.

In the present study, we examined the functional similarity and mutation status of nine hub genes: PTGS2, BCL2L1, ICAM1, MET, NQO1, MMP3, NFATC1, CCNB1 and ERBB3. We found significant positive correlations among these hub genes, with the strongest positive correlation observed between NQO1 and ERBB3 and the strongest negative correlation between NFATC1 and ERBB3. These findings suggest a possible synergistic or regulatory relationship among these genes in PAAD, which is important for a deeper understanding of its pathogenesis. Functional similarity analysis revealed that ERBB3 is a critical gene in PAAD, consistent with findings reported in previous studies (Hassan *et al*., 2022; Liu *et al*., 2021). These results provide valuable insights to guide further research on ERBB3's mechanisms, facilitating the development of therapeutic strategies for PAAD.

We performed immune infiltration analyses and found significant differences in the abundance of nine lymphocyte types between PAAD and normal tissues. These changes in infiltration suggest that these cells are involved in PAAD progression. Furthermore, immune analyses revealed that the expression of hub genes (ICAM1, MET, NQO1 and ERBB3) was positively related to Th2 and Th17 cells, which are immunosuppressive cells contributing to the tumor immune microenvironment (Stuanto *et al*., 2025; Ryba-Stanisławowska, 2025). Naive CD4+ T cells can differentiate into two subsets: Th1 cells, which promote proinflammatory responses and activate autoimmune processes and Th2 cells, which facilitate humoral immune responses via cytokines such as IL-4, IL-5, IL-9 and IL-10 (Zhu, 2018). The balance between Th1 and Th2 cells is disrupted in PAAD. Specifically, Th2 cells often remain at high levels, inducing inflammation and promoting tumor growth, which consequently leads to worse survival (Kao *et al*., 2025; Sadeghlar *et al*., 2021). Th17 cells secrete IL-17 and serve a crucial function in the immune modulation of tumors (Anvar *et al*., 2024; Pan *et al*., 2023). Evidence has shown that Th17 cells promote PAAD (Herting *et al*., 2021). Based on current literature and our findings, we hypothesize that these hub genes collaboratively interfere with the balance among Th1, Th2 and Th17 cells. This disruption results in a generally immunosuppressive microenvironment, which affects the prognosis of PAAD.

Additionally, drug sensitivity prediction showed that for 20 drugs with significant differences, PAAD patients in the high-risk cohort had higher IC50 values than those in the low-risk cohort, suggesting lower drug sensitivity in high-risk individuals. These findings indicate that low-risk patients treated with these agents are more likely to achieve better treatment responses and favorable outcomes. However, the pRRophetic model is trained on cell line data, which differs biologically from actual tumor tissues, particularly in terms of the tumor microenvironment and cellular heterogeneity. These differences may affect the accuracy of IC50 predictions for samples. Consequently, the prediction results primarily aim to identify potential trends and require further validation through functional experiments and clinical research.

There are several limitations in the present study. First, data integration involved multiple platforms. Although correction methods like SVA were applied, completely eliminating systematic biases remains challenging. It is recommended to introduce more advanced integration algorithms to improve data consistency. Second, despite implementing a cross-validation strategy with multiple datasets, potential bias from the limited sample size cannot be entirely eliminated. Therefore, results should be interpreted with caution and cross-validation using multiple datasets and methodologies is recommended. Future studies should aim to increase the number of normal tissue samples or integrate multi-center datasets to further validate and enhance the reliability and generalizability of the differential analysis results. Third, model construction was limited by sample size, posing a potential risk of overfitting. The model needs to be optimized by expanding

the sample size, applying cross-validation, and ensuring its robustness and application potential are validated in independent cohorts. Furthermore, these computational predictions require further validation through *in-vivo* and *in-vitro* experiments.

CONCLUSION

In summary, the present study assessed PAAD-related target genes involved in QYHJ treatment using network pharmacology and bioinformatics. Then, nine hub genes linked to PAAD treatment response and prognosis were identified. Several potential mechanisms involving modulation of inflammation, oxidative stress and apoptotic signaling pathways contribute to QYHJ therapy. The current results are merely computational predictions; thus, further integration of multi-omics data, functional experiments and prospective clinical validation are needed to refine these findings and facilitate their clinical translation.

Supplementary description
Table S1: Target genes list. Table S2: QYHJ for PAAD-related genes.

Acknowledgements
Not applicable.

Authors' contribution
Jiemin Shi: Study design, literature search, drafting, supervision and final approval; Jintao Han and Fuchu Qian: Data collection, literature search, drafting, data analysis, interpretations, writing and final approval. All authors have read and approved the final manuscript and are responsible for the integrity of the study.

Funding
This work was supported by the Foundation for Traditional Chinese Medicine Scientific Research of Zhejiang Province (2017ZA135) and the Medical and Health Research Project of Zhejiang Province (2025KY1545).

Data availability statement
The data generated and/or analyzed during the current study are available in the TCGA (The Cancer Genome Atlas) repository (https://portal.gdc.cancer.gov/) and GEO (https://www.ncbi.nlm.nih.gov/geo/) repository. The datasets are available in the project [TCGA-PAAD] AND the GEO under accession numbers GSE62452 and GSE57495.

Ethical approval
Not applicable.

Conflict of interest
The authors declare no conflict of interest.

Supplementary data
https://www.pjps.pk/uploads/2026/05/SUP1777635204.pdf

REFERENCES

Anvar MT, Rashidan K, Arsam N, Rasouli-Saravani A, Yadegari H, Ahmadi A, Asgari Z, Vanan AG, Ghorbaninezhad F and Tahmasebi S (2024). Th17 cell function in cancers: immunosuppressive agents or anti-tumor allies? *Cancer cell international.*, **24**(1): 355.

Chen NM, Neesse A, Dyck ML, Steuber B, Koenig AO, Lubeseder-Martellato C, Winter T, Forster T, Bohnenberger H, Kitz J, Reuter-Jessen K, Griesmann H, Gaedcke J, Grade M, Zhang JS, Tsai WC, Siveke J, Schildhaus HU, Strobel P, Johnsen SA, Ellenrieder V and Hessmann E (2017). Context-dependent epigenetic regulation of nuclear factor of activated t cells 1 in pancreatic plasticity. *Gastroenterology.,* **152**(6): 1507-1520.e15.

Chen NM, Singh G, Koenig A, Liou GY, Storz P, Zhang JS, Regul L, Nagarajan S, Kühnemuth B, Johnsen SA, Hebrok M, Siveke J, Billadeau DD, Ellenrieder V and Hessmann E (2015). NFATc1 Links EGFR Signaling to Induction of Sox9 transcription and acinar-ductal transdifferentiation in the pancreas. *Gastroenterology.*, **148**(5): 1024-1034.e9.

Chen P, Wang M and Wang C (2019). Qingyihuaji formula reverses gemcitabine resistant human pancreatic cancer through regulate lncRNA AB209630/miR-373/EphB2-NANOG signals. *Biosci Rep.*, **39**(6): BSR20190610.

Deng J, Guo Y, Hu X, Du J, Gu J, Kong L, Tao B, Fu D, Ying T and Li J (2022). High glucose promotes pancreatic ductal adenocarcinoma gemcitabine resistance and invasion through modulating ROS/MMP-3 signaling pathway. *Oxid Med Cell Longev.*, **2022**: 3243647.

Goldman MJ, Craft B, Hastie M, Repecka K, McDade F, Kamath A, Banerjee A, Luo Y, Rogers D, Brooks AN, Zhu J and Haussler D (2020). Visualizing and interpreting cancer genomics data via the Xena platform. *Nat Biotechnol.*, **38**(6): 675-678.

Guo D, Cheng K, Song C, Liu F, Cai W, Chen J, Mei Y, Zhou D, Gao S, Wang G and Liu Z(2023). Mechanisms of inhibition of nucleus pulposus cells pyroptosis through SDF1/CXCR4-NFkB-NLRP3 axis in the treatment of intervertebral disc degeneration by Duhuo Jisheng decoction. *Int Immunopharmacol.*, **124**(PtA): 110844.

Hassan G, Zahra MH, Seno A, Seno M (2022). The significance of ErbB2/3 in the conversion of induced pluripotent stem cells into cancer stem cells. *Sci Rep.*, **12**(1): 2711.

Herting CJ, Karpovsky and Lesinski GB (2021). The tumor microenvironment in pancreatic ductal adenocarcinoma: Current perspectives and future directions. *Cancer metastasis reviews.*, **40**(3): 675-689.

Jiao J, Cheng CS, Xu P, Yang P, Zhang K, Jing Y and Chen

Z (2022). Mechanisms of pancreatic tumor suppression mediated by Xiang-lian pill: An integrated in silico exploration and experimental validation. *J Ethnopharmacol.*, **298**: 115586.

Kao CJ, Charmsaz S, Alden SL, Brancati M, Li HL, Balaji A, Munjal K, Howe K, Mitchell S, Leatherman J, Griffin E, Nakazawa M, Tsai HL, Danilova L, Thoburn C, Gizzi J, Gross NE, Hernandez A, Coyne EM, Shin SM, Suresh Babu J, Apostol GW, Durham J, Christmas BJ, Konig MF, Lipson EJ, Naidoo J, Cappelli LC, Pabani A, Ged Y, Baretti M, Brahmer J, Hoffman-Censits J, Seiwert TY, Garonce-Hediger R, Guha A, Bansal S, Tang L, Jaffee EM, Chandler GS, Mohindra R, Ho WJ and Yarchoan M (2025). Immune-related events in individuals with solid tumors on immunotherapy associate with Th17 and Th2 signatures. *J Clin Invest.*, **135**(6): e192014.

Khalaf N, El-Serag HB, Abrams HR, Thrift AP (2021). Burden of pancreatic cancer: From epidemiology to practice. *Clin Gastroenterol Hepatol.*, **19**(5): 876-884.

Klein AP (2021). Pancreatic cancer epidemiology: Understanding the role of lifestyle and inherited risk factors. *Nat Rev Gastroenterol Hepatol.*, **18**(7): 493-502.

Lang J, Li L, Quan Y, Tan R, Zhao J, Li M, Zeng J, Chen S, Wang T, Li Y, Zhao J, Yin Z (2023). LC-MS-based metabolomics reveals the mechanism of anti-gouty arthritis effect of Wuwei Shexiang pill. *Front Pharmacol.*, **14**: 1213602.

Liu S, Cai Y, Changyong E, Sheng J and Zhang X (2021). Screening and validation of independent predictors of poor survival in pancreatic cancer. *Pathol Oncol Res.*, **27**:1609868.

Lux A, Kahlert C, Grützmann R and Pilarsky C (2019). c-Met and PD-L1 on circulating exosomes as diagnostic and prognostic markers for pancreatic cancer. *Int J Mol Sci.*, **20**(13): 3305.

Pan Y, Yang W, Tang B, Wang X, Zhang Q, Li W and Li L (2023). The protective and pathogenic role of Th17 cell plasticity and function in the tumor microenvironment. *Front Immunol.*, **14**: 1192303.

Park W, Chawla A and O'reilly EM (2021). Pancreatic cancer: A review. *JAMA.*, **326**(9): 851-862.

Qian X, Bi QY, Wang ZN, Han F, Liu LM, Song LB, Li CY, Zhang AQ and Ji XM (2023). Qingyihuaji formula promotes apoptosis and autophagy through inhibition of MAPK/ERK and PI3K/Akt/mTOR signaling pathway on pancreatic cancer *in-vivo* and *in-vitro*. *J Ethnopharmacol.*, **307**: 116198.

Qian X, Chen Z, Chen SS, Liu LM and Zhang AQ (2020) Integrated analyses identify immune-related signature associated with qingyihuaji formula for treatment of pancreatic ductal adenocarcinoma using network pharmacology and weighted gene co-expression network. *J Immunol Res.*, **2020**: 7503605.

Ritchie ME, Phipson B, Wu D, Hu Y, Law CW, Shi W and Smyth GK (2015). limma powers differential expression analyses for RNA-sequencing and microarray studies. *Nucleic Acids Res.*, **43**(7): e47.

Ryba-Stanisławowska M (2025). Unraveling Th subsets: Insights into their role in immune checkpoint inhibitor therapy. *Cell Oncol (Dordr).*, **48**(2): 295-312.

Ru J, Li P, Wang J, Zhou W, Li B, Huang C, Li P, Guo Z, Tao W, Yang Y, Xu X, Li Y, Wang Y and Yang L (2014). TCMSP: A database of systems pharmacology for drug discovery from herbal medicines. *J Cheminform.*, **6**: 13.

Sadeghlar F, Vogt A, Mohr RU, Mahn R, van Beekum K, Kornek M, Weismüller TJ, Branchi V, Matthaei H, Toma M, Schmidt-Wolf IGH, Kalff JC, Strassburg CP, Gonzalez-Carmona MA (2021). Induction of cytotoxic effector cells towards cholangiocellular, pancreatic and colorectal tumor cells by activation of the immune checkpoint CD40/CD40L on dendritic cells. *Cancer Immunol Immunother.*, **70**(5): 1451-1464.

Sayed AM, El-Hawary SS, Abdelmohsen UR and Ghareeb MA (2022). Antiproliferative potential of Physalis peruviana-derived magnolin against pancreatic cancer: A comprehensive *in-vitro* and *in-silico* study. *Food Funct.*, **13**(22): 11733-11743.

Shi W, Wang Z, Yu Z, Shen Y, Xin W and Chen W (2025). Qingyihuaji formula reprograms metabolism to suppress pancreatic cancer growth and progression through LINC00346-OMA1-ATF4 signaling. *J Ethnopharmacol.*, **348**: 119893.

Shi R, Sun T, Hua J, Yin S, Lv C, Gao Y, Lai K, Yu P and Chen X (2025). Qihuang Zhuyu formula mitigates cardiomyocyte apoptosis and hypertrophy via Bmal1-mediated P53 ubiquitination. *Phytomedicine.*, **148**: 157316.

Siegel RL, Miller KD, Wagle NS and Jemal A (2023). Cancer statistics, 2023. *CA Cancer J Clin.*, **73**(1): 17-48.

Sutanto H, Ningtyas MC, Rachma B, Pratiwi L and Fetarayani D (2025). Th17 cells in cancer: plasticity-driven immunopathology and therapeutic opportunity. *Immunol Cell Biol.*, **103**(7): 696-722.

Xiao C, Wang Y, Liu J, Li X, Wang P, Zhou J, Xiu H, Lu S, Zhu H and Wang R (2025). Mechanism of Fangji Huangqi decoction against acute kidney injury based on network pharmacology and experimental validation. *Phytomedicine.*, **136**:156345.

Xie J, Cheng JS, Zhu XY, Liu LM and Song LB (2020). Network pharmacology-based mechanism study of Qingyi Huaji recipe in treating pancreatic cancer. *Acad J Second Mil Med Univ.*, **41**: 1236-1245.

Yang PW, Xu PL, Cheng CS, Jiao JY, Wu Y, Dong S, Xie J and Zhu XY(2022). Integrating network pharmacology and experimental models to investigate the efficacy of QYHJ on pancreatic cancer. *J Ethnopharmacol.*, **297**: 115516.

Zeng Y and Fan R(2022). Identification and verification of CCNB1 as a potential prognostic biomarker by comprehensive analysis. *Sci Rep.*, **12**(1): 16153.

Zhang J, Liu X, Zhang G, Wu J, Liu Z, Liu C, Wang H,

Miao S, Deng L, Cao K, Shang M, Zhu Q and Sun P (2023). To explore the effect of kaempferol on non-small cell lung cancer based on network pharmacology and molecular docking. *Front Pharmacol.*, **14**: 1148171.

Zhang YL, Zhang X, Miao XZ, Yuan YY, Gao J, Li X, Liu YG and Tan P (2020). Coptisine suppresses proliferation and inhibits metastasis in human pancreatic cancer PANC-1 cells. *J Asian Nat Prod Res.*, **22**(5): 452-463.

Zhang Z, Wang X, Hamdan FH, Likhobabina A, Patil S, Aperdannier L, Sen M, Traub J, Neesse A, Fischer A, Papantonis A, Singh SK, Ellenrieder V, Johnsen SA and Hessmann E (2023). NFATc1 is a central mediator of EGFR-induced ARID1A chromatin dissociation during acinar cell reprogramming. *Cell Mol Gastroenterol Hepatol.*, **15**(5): 1219-1246.

Zhou J, Hui X, Mao Y and Fan L (2019). Identification of novel genes associated with a poor prognosis in pancreatic ductal adenocarcinoma via a bioinformatics analysis. *Biosci Rep.*, **39**(8): BSR20190625.

Zhu J (2018). T helper cell differentiation, heterogeneity and plasticity. *Cold Spring Harb Perspect Biol.*, **10**(10): a030338.